Strongly correlated physics in organic open-shell quantum systems

G. Gandus, ^{1,*} A. Jayaraj, ^{2,*} D. Passerone, ² R. Stadler, ³ M. Luisier, ¹ and A. Valli^{4,5,†}

¹ Integrated Systems Laboratory, ETH Zürich, Gloriastrasse 35, 8092 Zürich, Switzerland

² Empa, Swiss Federal Laboratories for Materials Science and Technology,

Überlandstrasse 129, CH-8600, Dübendorf, Switzerland

³ Institute for Theoretical Physics, Vienna University of Technology,

Wiedner Hauptstrasse 8-10, A-1040 Vienna, Austria

⁴ Department of Theoretical Physics, Institute of Physics,

Budapest University of Technology and Economics, Műegyetem rkp. 3., H-1111 Budapest, Hungary

⁵ HUN-REN-BME-BCE Quantum Technology Research Group,

Budapest University of Technology and Economics, Műegyetem rkp. 3., H-1111 Budapest, Hungary

Strongly correlated physics arises from electron-electron scattering within partially filled orbitals. Organic molecules in open-shell configurations are therefore good candidates to exhibit many-body effects. We focus on electron transport in a two-terminal single-molecule junction setup, in which the molecular bridge consists of an organic radical with a molecular orbital hosting a single unpaired electron (SOMO). We perform beyond state-of-the-art numerical simulations combining an *ab-initio* description of the chemical environment, with quantum field-theoretical techniques that account for many-body effects. The key observation is that the SOMO resonance is prone to splitting and we identify a *giant* electronic scattering rate as the driving many-body mechanism, akin to that of the Mott metal-to-insulator transition. By comparing linear and cyclic radicals, we show that the spatial distribution of the SOMO and its projection on the molecular backbone have dramatic consequences for the transport properties of the junction. We argue that the phenomenon and the underlying microscopic mechanism apply to a broad family of open-shell molecular systems, and can explain puzzling experimental observations such as suppressed conductance in radical junctions.

I. INTRODUCTION

Strongly correlated electronic physics emerges in partially occupied orbitals in the presence of competing energy scales. The concept of a "strongly-correlated metal" is well established, and refers to materials in which mutual Coulomb repulsion among electrons leads to collective behavior, causing the breakdown of the singleparticle approximation and the emergence of complex quantum phenomena. Extending this idea to molecular systems, characterized by discrete energy levels, is not obvious. Most stable organic molecules exhibit closedshell electronic configurations, with valence electrons of opposite spin paired such that molecular orbitals (MOs) are either empty or filled. Radical molecules, however, are an exception to this pattern, characterized by (at least) one unpaired valence electron residing in nonbonding, singly-occupied MOs (SOMOs). Thus, radicals realize open-shell electronic configurations, and are therefore natural candidates to exhibit strong correlation

Neutral radicals can form through bond cleavage or electron transfer and often appear as intermediate products of chemical reactions. The presence of unpaired electrons in the outer shell makes them inherently unstable. Tremendous advances in the synthesis and characterization of radicals [1–3] have enabled the isolation of persistent radical species that, despite their high chemical re-

activity, remain stable long enough to be trapped in the nanogap of mechanically-controlled break-junctions [4– 18] or deposited onto substrates [19–22]. This has facilitated the investigation of their electronic properties via transport spectroscopy. Interest in such systems has grown rapidly, driven by observations of radicals exhibiting remarkable electronic [4–6, 23, 24], magnetic [12, 25– 27], and optical [28–30] functionalities. These properties are relevant to emerging technologies ranging from nextgeneration nano-electronics [1], to spintronics [2, 25, 31-33], sensing [34, 35], and quantum information [36, 37]. In the context of molecular electronics, noteworthy organic radicals include triphenylmethyl [4, 26, 38, 39], nitroxide [8, 18, 40], triazine [6, 19, 41, 42], and benzyl [25, 43, 44] derivatives, odd-numbered polyacetylene chains [45, 46], and polycyclic hydrocarbons with non-Kekulé structure [11, 20, 21, 33, 47–49]. Molecular organic frameworks (such as porphine and phthalocyanine) hosting transition-metal centers, are typically in open-shell configuration and many-body effects have been shown to play a pivotal role in realizing tunable molecular transistors [50, 51].

A natural question arises as to whether an organic radical retains its open-shell configuration in a solid-state device. Recent theoretical investigations of nitroxyl radicals suggest that, despite non-trivial interactions with Au electrodes, [40] the open-shell character is robust against interactions with the solvent molecules or under applied bias [42]. However, the experimental situation is seemingly controversial, as radicals appear to exhibit environment-dependent behavior [19]. Clear evidence of a zero-bias resonance has been reported in organic rad-

^{*} These authors contributed equally to this work

[†] valli.angelo@ttk.bme.hu

ical two-terminal junctions with the molecule bonding to metal electrodes [6, 18, 26] or adsorbed on a surface [10, 13, 14], and ascribed to the quenching of the unpaired electrons due to the Kondo effect. Although, in some cases, organic radicals have been shown to demonstrate enhanced conductance [5, 7] and Seebeck coefficient [5] relative to their non-radical counterparts, the reported conductance values [5, 7, 19] are typically of the order of $G \sim 10^{-3} G_0$. This is significantly lower than the expected value for a fully open transport channel exhibiting nearly resonant transmission through a low-lying molecular orbital, where $G \sim G_0 = e^2/h$. Moreover, conductance traces reported for a (Blatter) triazinyl radical in a break-junction setup closely resembled those of an oxidized derivative, with conductance comparable to that of closed-shell stilbene, thereby suggesting that the openshell character is lost in certain device configurations [19].

This apparent discrepancy raises the question: is the loss of radical character the only explanation for the suppressed conductance observed experimentally? We argue that a possible alternative explanation can be ascribed to many-body effects. In organic (semiconducting) molecules and nano-structures, the electron-electron scattering rate is low due to the lack of electronic states close to the Fermi energy, and electronic correlations manifest in other ways. For instance, the failure of ab-initio simulations in reproducing the correct HOMO-LUMO gap is a long-standing issue [52], and numerical simulations predict a many-body renormalization of the single-particle gap [53–62]. Another hallmark of electron correlation is the Coulomb blockade phenomenon, which has been experimentally observed in organic molecular junctions [63–68] and graphene nanoribbons [69, 70], in the regime where the charging energy dominates over the molecule-electrodes coupling. In contrast, molecules in open-shell configurations are expected to exhibit significant electron-electron scattering within the partially filled SOMO. In computational quantum chemistry, it is well-established that open-shell molecular configurations require careful treatment (see, e.g., [71] for an overview) but the accuracy of quantum chemical methods comes at a prohibitively high numerical cost. Despite significant advances in simulation schemes for complex molecular and nano-electronic devices [39, 59, 60, 72– 76, investigations of organic radicals within genuinely many-body frameworks (i.e., beyond static mean-field) remain limited. Moreover, they mostly focus either on Kondo physics [6, 39, 44, 77–80]—relevant at low (cryogenic) temperatures, or on understanding intermolecular exchange couplings [21, 48, 81, 82], whereas the high-temperature phenomenology (i.e., above the Kondo scale) of stable and persistent organic radicals remains largely unexplored.

In the following, we focus on the electron transport in a two-terminal single-molecule junction configuration, in which an organic radical bridges metallic electron reservoirs. Specifically, we select a linear (pentadienyl) and a cyclic (benzyl) radical as archetypal representatives, since both molecules are π -radicals with a single unpaired electron, and natural candidates to manifest many-body effects

Our key result is to show that the Coulomb repulsion within the SOMO induces a many-body splitting of the SOMO resonance. We suggest this scenario as a possible explanation for the relatively low conductance observed in transport experiments. In particular, we (i) identify the splitting as the hallmark of strong electron correlations, (ii) pinpoint the origin of the splitting, ascribed to a giant electron scattering rate within the SOMO, and (iii) demonstrate that the phenomenology of the splitting is a non-perturbative effect of the Coulomb repulsion, and cannot be obtained with less sophisticated techniques, such as perturbative approaches or static mean-field theories.

We argue that the splitting of the SOMO is a general phenomenon that applies to a broad family of open-shell molecular systems, but at the same time, we highlight how a different spatial distribution of the SOMO bears dramatic consequences for the transport properties of the junction. Finally, we discuss its relevance in transport experiments and suggest a non-linear current-voltage characteristics as a possible experimental probe to confirm our predictions.

II. METHODS

We have developed a comprehensive numerical workflow that combines density functional theory (DFT) with quantum field theoretical methods, and is therefore able to address the chemical complexity of the radical molecule *ab-initio* as well as electronic correlation effects beyond the single-particle picture. In the following, we discuss each building block and how they come together to provide a comprehensive and reliable framework to investigate the electronic and transport properties of strongly correlated molecule junctions.

A. Local orbitals and low-energy models

The art of combining ab-initio and many-body approaches is to find a minimal orthogonal basis set, which describes the correlated manifold. Maximally localized Wannier functions (WFs) [83] are routinely used in this context. However, due to their variational nature, WFs are not ideal in the context of quantum transport, as they require separate calculations for the scattering region and the electrodes. To date, there has been an ongoing effort to ease key challenges, including, for example, the automated generation of WFs [84] and interface matching [85]. Variations of WFs, particularly suitable for molecules, have also been proposed [86].

We follow an alternative approach relying on a linear combination of atomic orbitals (LCAO). At the heart of the proposed computational scheme lies a unitary transformation from the non-orthogonal atomic orbitals (AOs) used in the DFT calculation to a basis that reflects the local chemical environment of each atom in the molecule [87, 88]. Following [88], we refer to the rotated basis as local orbitals (LOs). So far, the LO approach has been employed in the context of DFT, for instance, to separate the contributions of the σ and π systems to the transmission function [87, 89, 90], and to perform electron transport simulations very efficiently. without sacrificing numerical accuracy [88]. In what follows, we rely on the LOs approach in combination with quantum embedding to map the original Hamiltonian in the AO basis to an effective many-body problem in which the correlated active space, with hopping and Coulomb integrals evaluated in the LO basis, is embedded in a space representing the rest of the system. The effective problem can then be solved with appropriate numerical methods. This framework provides a comprehensive theoretical tool with predictive power, particularly suited for addressing the transport properties of molecular and nano-junctions.

The starting point is a DFT calculation in an AO basis set, within the LCAO scheme, leading to a finite set of non-orthogonal Kohn-Sham orbitals $\{|i\rangle\}$ that span the Hilbert space H, with overlap matrix $\langle i|j\rangle = (\mathbf{S})_{ij} \neq \delta_{ij}$ for $|i\rangle, |j\rangle \in H$. A set of LOs $\{|m\rangle\}$, with $|m\rangle \in M \subseteq H$ can be obtained for any atom α in subspace M by a subdiagonalization of the corresponding Hamiltonian sub-block

$$\mathbf{H}_{\alpha} \left| m \right\rangle = \epsilon_m \mathbf{S}_{\alpha} \left| m \right\rangle. \tag{1}$$

The LOs are therefore linear combinations of AOs and are, by construction, orthogonal on each atom. They can be classified according to symmetry, devoid of the redundancy characteristic of split-valence basis sets. This enables a more natural physical interpretation of the LOs as atomic orbitals [88].

To obtain an effective model ab-initio, we formally separate the Hilbert space into an active space (A) and an environment (E). The active space consists of a subset of LOs $\{|a\rangle\}$, with $|a\rangle \in A \subseteq M$ which are expected to describe the physics close to the Fermi energy, and, at the same time, can be feasibly treated within quantum many-body techniques. The environment consists of all the remaining LOs and AOs $\{|e\rangle\}$, with $|e\rangle \in E \equiv H \setminus A$. Embedding the active space into the environment (rather than neglecting it) ensures that the effective model retains all information from the original single-particle Hamiltonian [88]. Finally, it is convenient to perform a Löwdin orthogonalization [91] of the set of LOs $\{|a\rangle\}$, so that the active region A is spanned by an orthonormal basis with elements

$$|a^{\perp}\rangle = \sum_{a} (\mathbf{S}^{-1/2})_{aa^{\perp}} |a\rangle.$$
 (2)

Since the overlap between LOs belonging to different atoms is typically small, i.e., $(\mathbf{S})_{ij} = \langle m_i | m_j \rangle \ll 1$, the

Löwdin orthonormalization of the active space introduces only a weak deformation of the original LOs, thus preserving their (approximate) atomic-like symmetry.

In practice, the (Löwdin) LO low-energy model is constructed by embedding the active subspace into the environment through a downfolding procedure [92, 93]. Taking into account the non-orthogonality between the A and E subspaces [73], the Green's function projected onto the A subspace is given by

$$\mathbf{G}_A(z) = \mathbf{S}_A^{-1} \mathbf{S}_{AH} \mathbf{G}_H(z) \mathbf{S}_{HA} \mathbf{S}_A^{-1}, \tag{3}$$

where $z = E + i\eta$ is a complex energy with an infinitesimal shift $\eta \to 0^+$. \mathbf{G}_H denotes the Green's function of the full Hilbert space, and \mathbf{S}_{AH} the overlap matrix between orbitals $|a^{\perp}\rangle \in A$ and orbitals $|i\rangle \in H$. Since the overlap \mathbf{S}_A between the $|a^{\perp}\rangle$ states is the identity matrix by construction, it will be omitted in what follows for notational simplicity. The effect of the environment on the A subspace is described by the hybridization function

$$\mathbf{\Delta}_A(z) = \mathbf{g}_A^{-1}(z) - \mathbf{G}_A(z)^{-1},\tag{4}$$

where

$$\mathbf{g}_A = \left[z - \mathbf{H}_A \right]^{-1} \tag{5}$$

is Green's function of the isolated A subspace. Rewriting G_A in terms of Δ_A and using the definition of g_A yields

$$\mathbf{G}_A(z) = \left[z - \mathbf{H}_A - \mathbf{\Delta}_A(z)\right]^{-1}.$$
 (6)

Then, \mathbf{G}_A can be seen as the resolvent operator for an effective A subspace renormalized by the environment through a dynamical hybridization. The Green's function describes the physics of the whole system, projected onto the active subspace.

For a single-particle Hamiltonian, the partition above is arbitrary, and the procedure remains valid regardless of the subset of LOs included in the active space. In the context of π -conjugated organic molecules, the projection onto a single LO with p_z symmetry per C atom (and, where relevant, additional species such as N or S) is usually sufficient to achieve a faithful representation of the frontier MOs, This choice is hence suitable to describe the physics close to the Fermi energy [88], but more LOs can be included if required. The possibility of considering a restricted subset of LOs in the effective model is of pivotal importance in view of performing computationally-heavy many-body simulations.

B. cRPA and ab-initio Coulomb parameters

In order to derive the electronic interaction parameters in the A subspace beyond the semi-local density approximations, we employ the constrained Random Phase Approximation (cRPA) [73, 94, 95]. Within the cRPA, we select a region $R \supset A$ where the formation of electronhole pairs is expected to screen the Coulomb interaction

between the A electrons. Due to the strong local nature of the LOs, it is sufficient that R comprises the A subspace and a few atoms nearby [73]. Defining \mathbf{G}_R to be the Green's function projected onto the R subspace, in analogy with Eq. (3), the screened Coulomb interaction is given by

$$\mathbf{W}_{R}(z) = \left[\mathbf{I} - \mathbf{V}_{R} \mathbf{P}_{R}(z)\right]^{-1} \mathbf{V}_{R},\tag{7}$$

where \mathbf{V}_R is the bare Coulomb interaction

$$\mathbf{V}_{R;ij,kl} = \int \! dr \int \! dr' \psi_i(r) \psi_j^*(r) \frac{e^2}{|r - r'|} \psi_k^*(r') \psi_l(r'),$$
(8)

with $\psi_i(r)$ the wavefunction of the corresponding orbital in the R region, and \mathbf{P}_R the polarizability at the RPA level

$$\mathbf{P}_{R;ij,kl}(z) = -2i \int \frac{dz'}{2\pi} \mathbf{G}_{R;ik}(z-z') \mathbf{G}_{R;lj}(z').$$
 (9)

The projection of \mathbf{W}_R onto the A subspace then yields the screened interaction \mathbf{W}_A . Since we aim at performing many-body simulations of the effective model, we need to partially unscreen the Coulomb parameters by eliminating from \mathbf{W}_A the screening channels arising from A-Atransitions included in \mathbf{P}_R . These contributions will instead be treated at a more sophisticated level of theory. This can be done according to the following prescription

$$\mathbf{U}_A(z) = \mathbf{W}_A(z) \left[\mathbf{I} + \mathbf{P}_A(z) \mathbf{W}_A(z) \right]^{-1}, \quad (10)$$

using the polarization \mathbf{P}_A of the A electrons obtained from \mathbf{G}_A similarly to Eq. (9). The static components $\mathbf{U}_A(z=0)$ are the (partially screened) Coulomb parameters in the active space.

C. Solutions of the low-energy models

The Green's function of Eq. (6), and the interactions parameters of Eq. (10), define a low-energy model in the LO basis that can be solved with many-body techniques. Here, we propose two somewhat complementary strategies based on exact diagonalization (ED) and dynamical mean-field theory (DMFT) [96] as implemented within its real-space generalization (R-DMFT) for inhomogeneous systems [72, 97–99].

1. Exact diagonalization

The ED technique requires a Hamiltonian formulation of the effective model. A possibility is to neglect the dynamical character of the hybridization function and construct an effective Hamiltonian as

$$\mathbf{H}_A^{\text{eff}} = \mathbf{H}_A + \operatorname{Re} \mathbf{\Delta}_A(z=0), \tag{11}$$

where the hybridization term accounts for a renormalization of the hopping amplitudes and orbital energies within the active space due to the embedding. This is a reasonable approximation if the states of the active and embedding subspaces are energetically well-separated and/or the density of states of the embedding subspace is smooth around the Fermi energy. The model Hamiltonian then reads

$$H = \sum_{ij,\sigma} \left[\mathbf{H}_{A}^{\text{eff}} - \mathbf{H}_{A}^{\text{dc}} \right]_{ij} c_{i\sigma}^{\dagger} c_{j\sigma}$$

$$+ \frac{1}{2} \sum_{ijkl,\sigma\sigma'} \mathbf{U}_{A;ij,kl} c_{j\sigma}^{\dagger} c_{k\sigma'}^{\dagger} c_{l\sigma'} c_{i\sigma},$$

$$(12)$$

where $c_{i\sigma}^{(\dagger)}$ denotes the annihilation (creation) operator of an electron at LO i with spin σ , \mathbf{U}_A is the matrix of the cRPA screened Coulomb interaction parameters, and the double-counting correction $\mathbf{H}_A^{\mathrm{dc}}$ accounts for the interaction already included at the mean-field level within DFT (see Sec. II D for the details). The diagonalization of this Hamiltonian yields its many-body spectrum (i.e., eigenorbitals and eigenvalues) which can be used to construct the Green's function $\mathbf{G}_A^{\mathrm{ED}}$ through its Lehmann representation [100]. The many-body self-energy is obtained from the Dyson equation

$$\Sigma_A^{\text{ED}}(z) = z - \mathbf{H}_A^{\text{eff}} - \left[\mathbf{G}_A^{\text{ED}}(z) \right]^{-1}, \tag{13}$$

and it describes local $\Sigma_{A;ii}$ and non-local $\Sigma_{A;i\neq j}$ electronic correlations in the LO basis. While ED is limited to $\mathcal{O}(20)$ orbitals, an obvious advantage over approaches such as quantum Monte Carlo [101], is that ED provides direct access to the retarded self-energy and Green's function (and therefore also to the transmission function) without the need to perform a numerical analytic continuation, which is known to be an ill-defined problem [102]. Note that within ED, we obtain a many-body self-energy which is, by construction, spin-independent, i.e., $\Sigma_{ij}^{\sigma} = \Sigma_{ij}^{\bar{\sigma}}$ since $\mathbf{H}_A^{\text{eff}}$ follows from a restricted DFT calculation.

2. Real-space DMFT

The idea behind R-DMFT consists of mapping the many-body problem onto a set of auxiliary Anderson impurity models (AIMs) —one for each atom α — described by the projected Green's function [97–99]

$$\mathbf{g}_{\alpha}^{\sigma}(z) = \left[\mathbf{G}_{A}^{\sigma}(z)\right]_{\alpha}.\tag{14}$$

The solution of AIM α yields a local many-body self-energy $\Sigma_{\alpha}^{\sigma}(z)$. Therefore, the self-energy of the A subspace is block diagonal in the atomic subspaces

$$\Sigma_A^{\sigma}(z) = \operatorname{diag}(\{\Sigma_{\alpha}^{\sigma}(z) \mid \alpha \in A\}). \tag{15}$$

The auxiliary AIMs are coupled by the Dyson equation

$$\mathbf{G}_{A}^{\sigma}(z) = \left[z + \mu - (\mathbf{H}_{A} - \mathbf{H}_{A}^{\mathrm{dc}}) - \boldsymbol{\Delta}_{A}(z) - \boldsymbol{\Sigma}_{A}^{\sigma}(z)\right]^{-1}, (16)$$

where the Green's function \mathbf{G}_A^{σ} includes the many-body self-energy and the double-counting correction (see Sec. II D for the details). The chemical potential μ can either be determined self-consistently to fix the total occupation of the active space (e.g., to preserve the DFT occupation of the A subspace) or set to a predefined value. Finally, Eqs. (14-16) are iterated self-consistently starting from an initial guess (typically the uncorrelated solution with $\mathbf{\Sigma}_A^{\sigma}=0$) until convergence.

In more detail, in AIM α the impurity electrons interact through a screened local Coulomb repulsion projected onto atom α , i.e., $\mathbf{U}_{\alpha} = \mathbf{U}_{A;ij,kl} \mid \{i,j,k,l\} \in \alpha$ [103]. Moreover, the impurity is embedded in a self-consistent bath of non-interacting electrons, which describes the rest of the electronic system, encoded in the hybridization function

$$\Delta_{\alpha}^{\sigma}(z) = z + \mu - (\mathbf{H}_{\alpha} - \mathbf{H}_{\alpha}^{\mathrm{dc}}) - \left[\mathbf{g}_{\alpha}^{\sigma}(z)\right]^{-1} - \Sigma_{\alpha}^{\sigma}(z). \tag{17}$$

Also within R-DMFT, it is convenient to use an ED impurity solver for the AIMs to have direct access to retarded functions. This requires a discretization of the hybridization function with a finite number of bath orbitals, described by orbital energies ϵ_m^{σ} and hopping parameters to the impurity orbital t_{mi}^{σ} . The hybridization parameters together with the local Coulomb blocks \mathbf{U}_{α} , define the AIM Hamiltonian

$$\begin{split} H_{\text{AIM}} &= \sum_{ij,\sigma} \left[\mathbf{H}_{\alpha} - \mathbf{H}_{\alpha}^{\text{dc}} \right]_{ij} c_{i\sigma}^{\dagger} c_{j\sigma} - \mu \sum_{i\sigma} c_{i\sigma}^{\dagger} c_{i\sigma} \\ &+ \sum_{m,\sigma} \epsilon_{m}^{\sigma} a_{m\sigma}^{\dagger} a_{m\sigma} + \sum_{mi,\sigma} t_{mi}^{\sigma} (a_{m\sigma}^{\dagger} c_{i\sigma} + c_{i\sigma}^{\dagger} a_{m\sigma}) \\ &+ \frac{1}{2} \sum_{ijkl,\sigma\sigma'} \mathbf{U}_{\alpha;ij,kl} c_{j\sigma}^{\dagger} c_{k\sigma'}^{\dagger} c_{l\sigma'} c_{i\sigma}, \end{split}$$

$$(18)$$

where $c_{i\sigma}^{(\dagger)}$ and $a_{m\sigma}^{(\dagger)}$ denote the annihilation (creation) operator of an electron at LO $i \in \alpha$ with spin σ , or at bath orbital m with spin σ , respectively. Once the manybody spectrum of the AIM is known, the local self-energy is evaluated in terms of the local Green's function $\mathbf{G}_{\alpha}^{\sigma}$ as

$$\Sigma_{\alpha}^{\sigma}(z) = \left[\mathbf{g}_{\alpha}^{\sigma}(z) \right]^{-1} - \left[\mathbf{G}_{\alpha}^{\sigma}(z) \right]^{-1}, \tag{19}$$

and Σ_A^{σ} according to Eq. (15). At convergence, we define the R-DMFT self-energy as

$$\Sigma_A^{\sigma, R-DMFT}(z) = \Sigma_A^{\sigma}(z) - \mathbf{H}_A^{dc} - \mu,$$
 (20)

so that it includes all shifts associated with the density matrix.

In terms of approximations, R-DMFT accounts for local electronic correlations $(\Sigma_{A;ii})$, while neglecting non-local correlations (i.e., $\Sigma_{A;i\neq j}=0$). However, some degree of non-locality is retained since $\Sigma_{A;ii} \neq \Sigma_{A;jj}$, as the AIMs are coupled self-consistently through the Dyson equation. R-DMFT is therefore suitable to describe electronic correlations in intrinsically inhomogeneous systems [55, 72, 99, 104–106]. Moreover, the computational complexity of R-DMFT is exponential in the

number of LOs in each atom α but only linear in the number of atoms. Since the AIMs are defined by Eq. (14) are independent, this also allows (i) exploiting any real-space symmetry of the many-body Hamiltonian, and solve only the locally inequivalent AIMs, and (ii) parallelizing the solution of said impurity problems. Therefore, R-DMFT is considerably lighter than direct ED of the original many-body problem in terms of computational complexity, and can treat systems with hundreds of atoms in the active space [55, 97, 99]. Finally, beyond the restricted solution $\Sigma_A^{\sigma} = \Sigma_A^{\bar{\sigma}}$, R-DMFT also permits breaking spin degeneracy and thus describing magnetic solutions with short-range order [57, 59, 60, 97, 107].

D. Double-counting correction

The double-counting (DC) correction \mathbf{H}_A^{dc} aims at eliminating the electron-electron correlations in the A subspace accounted for at mean-field level in the DFT calculation, which will be replaced by those obtained at a more sophisticated level of theory in the many-body simulations. Unfortunately, since DFT (in contrast to, e.g., GW) does not have a formulation in terms of Feynman diagrams, the analytical expression of such a correction within DFT is unknown. Several approximations [72, 108–110] have been developed in the context of DFT+U [111, 112] or DFT+DMFT [113, 114]. Here, we choose the fully localized limit (FLL) [109, 115–117] generalized to the case of an anisotropic Coulomb repulsion [73]. For a single correlated orbital per atom in the correlated subspace (as in the case of the simulations in this work) this reduces to

$$\mathbf{H}_{A;ii}^{\mathrm{dc}} = \mathbf{U}_{A;ii,ii} \left(n_i^{\mathrm{DFT}} - \frac{1}{2} \right), \tag{21}$$

where n_i^{DFT} is the DFT occupation of orbital i. Hence, we use this form of DC for the R-DMFT calculations. However, there's no established method for the general case of multi-site and multi-orbital Coulomb interaction as encountered in ED. A possible choice is to require the correlated self-energy to fulfill the condition [118]

$$\operatorname{Re}\operatorname{Tr}\left[\mathbf{\Sigma}_{A}(|z|\to\infty)\right] = 0,\tag{22}$$

which we implement here within a self-consistent procedure optimizing a set of local parameters that play the role of effective orbital occupations in Eq. (21). This approach ensures that the electronic properties at high energies, which are well described by a one-particle approach, are restored (on average) to the DFT level.

E. Correlated quantum transport

To describe the electronic transport properties, we use the non-equilibrium Green's function (NEGF) approach [119, 120]. In NEGF, we identify a device region that extends beyond the molecular bridge, and downfold the leads' electrons by virtue of an efficient recursive algorithm [121]. The corresponding Green's function reads

$$\mathbf{G}_{D}(z) = \left[z \mathbf{S}_{D} - \mathbf{H}_{D} - \boldsymbol{\Sigma}_{L}(z) - \boldsymbol{\Sigma}_{R}(z) - \boldsymbol{\Sigma}_{D}(z) \right]^{-1}, (23)$$

where $\Sigma_{L(R)}$ is the self-energy describing the electrons in the left (right) electrodes, and

$$\Sigma_D(z) = \mathbf{S}_{DA} \mathbf{S}_A^{-1} \Sigma_A(z) \mathbf{S}_A^{-1} \mathbf{S}_{AD}$$
 (24)

projects the many-body self-energy of the active space Σ_A (i.e., obtained within either ED or R-DMFT) onto the device region. Following the generalization of the Landauer formula proposed by Meir and Wingreen [122], the conductance is given by

$$G = G_0 T(E_F), (25)$$

where $G_0 = e^2/h$ is the conductance quantum, and the transmission function is computed as

$$T(E) = \text{Tr}[\mathbf{\Gamma}_L(z)\mathbf{G}_D^{\dagger}(z)\mathbf{\Gamma}_R(z)\mathbf{G}_D(z)], \qquad (26)$$

with $\Gamma_{L(R)}$ the anti-hermitian part of $\Sigma_{L(R)}$

$$\Gamma_{L(R)}(z) = i \left[\mathbf{\Sigma}_{L(R)}(z) - \mathbf{\Sigma}_{L(R)}^{\dagger}(z) \right]. \tag{27}$$

Note that Eqs. (25)-(27) neglect the incoherent contributions (i.e., due to inelastic scattering) to the transmission that arise from the many-body self-energy [74, 75, 122–126]. In the non-resonant transport regime, and where electron-electron scattering is low, a Landauer transmission with renormalized Green's functions is expected to provide a good approximation of the transport properties at low bias voltage, even in the presence of strong correlations within the A subspace [73, 122].

However, it can be shown that the transmission can be recast as

$$T(E) = \text{Tr}[\mathbf{\Gamma}_L(z)\mathbf{G}_D^{\dagger}(z)\mathbf{\Lambda}_R(z)\mathbf{G}_D(z)], \qquad (28)$$

so that correlation effects are included in a effective (renormalized) coupling to one of two electrodes

$$\Lambda_R(z) = \Gamma_R(z) + \Gamma_c(z). \tag{29}$$

Hence, the transmission function it is naturally separated in two contributions: (i) a bubble term that reduces to the Landauer transmission as $\Lambda_R(z) \to \Gamma_R(z)$, and (ii) a vertex correction arising from $\Gamma_c(z)$, that takes into account inelastic electron scattering. The calculation of the vertex correction requires either the knowledge of a vertex function [127] or of the non-equilibrium distribution of the electrons in the presence of interactions [122–125]. While this goes beyond the scope of the present work, we note that in the literature, different approximate recipes have been proposed to tackle this problem. [124, 126–128].

III. COMPUTATIONAL DETAILS

The structures were set up with the atomic simulation environment (ASE) software package [129] and the DFT calculations were performed with the GPAW package [130–132]. Geometry optimizations were performed by relaxing atomic positions until the forces on each atom were below 0.001 Hartree/Bohr⁻¹ ($\approx 0.05 \text{ eV/Å}$). To converge the electron density, we used an LCAO double- ζ basis set, with a grid spacing of 0.2 Å, and the Perdew–Burke–Ernzerhof exchange-correlation functional [133]. The leads were modeled by a three-layer-thick Au(111) slab sampled with a $3 \times 1 \times 1$ k-point grid along the transport direction. The scattering region also includes one Au slab and an additional Au layer terminated by a four-atom Au tip, to which the molecule anchoring groups are attached.

For all structures considered below, the A subspace describing the effective model consists of the p_z LOs of the C and N atoms of the molecular bridge [121], while the R subspace for the cRPA calculation of the screened interaction includes the molecule and also extends to the Au atoms of the tip (see Fig. 1).

The R-DMFT simulations were performed with and ED impurity solver [134, 135] converging the solution with up to $n_b=7$ bath sites discretization for each AIM. The ED simulations we performed using edpyt [136]. In both cases we choose to set $\mu=0$ so that the Fermi energy is determined by the electron reservoirs in the junction (which is the reference energy of the AO Hamiltonian) and recalculate the occupation of the active space self-consistently. The quantum transport NEGF simulations without and with a many-body self-energy were performed using qtpyt [137].

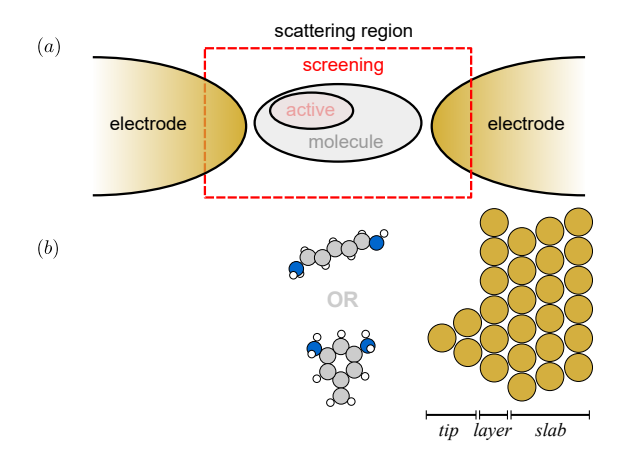


Figure 1. (a) Schematics of the scattering region of the single-molecule junction, consisting of the molecular bridge and the Au electrodes. The screening space (R) and active space (A) intended as a subspace of the orbitals of the molecule, are highlighted. (b) Structure of the pentadienyl and benzyl radicals, substituted with the amino anchoring groups, and of the Au(111) electrodes.

IV. INSIGHTS FROM AB-INITIO SIMULATIONS

To understand the many-body effects arising in an open-shell configuration, it is useful to recall relevant chemical properties of the parent radicals and show how those are reflected in their substituted counterparts in the junction setup from *ab-initio* simulations. In particular, we inspect the spatial distribution of the SOMO and the cRPA Coulomb parameters projected onto the LOs active space.

A. Structure of the SOMO

The pentadienyl radical, with the chemical formula $[CH_2(CH)_3CH_2]^z$ (with total charge z=0), is a linear molecule and the shortest polyene radical after allyl. It has three resonant structures, in each of which the unpaired electron is hosted on one of the odd C atoms. The delocalization of the unpaired electron along the molecular backbone contributes to the thermodynamic stability of the molecule [138, 139]. In the junction setup, the hydrogen atoms at each end of the chain are substituted by amino anchoring groups. By diagonalization of the AOs Hamiltonian, restricting to the subspace of the molecule, we obtain the corresponding fragment MOs, and we find an eigenvalue just above the Fermi energy, corresponding to the SOMO. The SOMO reflects the resonant structures, with its largest projection on the odd carbon atoms, nodes on the even ones, and a significant weight on the anchoring groups - indicating strong coupling to the electrodes. The pentadienyl resonant structures, the substituted molecule, and the projection of the SOMO onto the p_z LOs of the active space are shown in Figs. 2(a,b,c), respectively.

The benzyl radical, $[C_6H_5CH_2]^z$ (with total charge

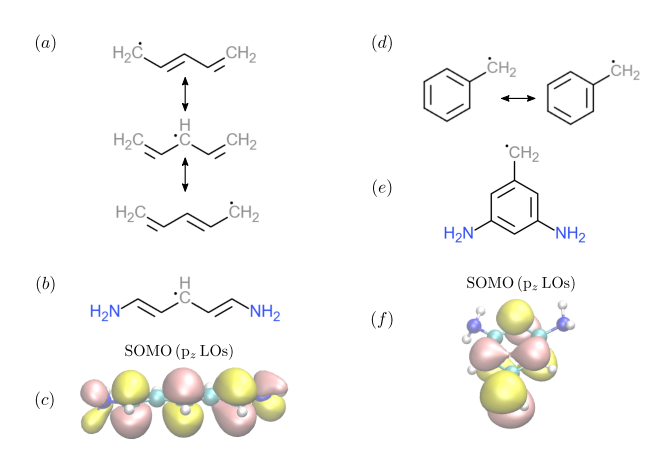


Figure 2. (a,d) Resonant structures of the pentadienyl and benzyl radicals in the gas phase. (b,e) Structure of the radical molecules substituted with amino anchoring groups. (c,f) SOMO isosurfaces projected on the p_z LOs of the substitued molecules. Isovalues: ± 0.03 au. See text for a discussion.

z=0), is derived from benzene (C₆H₆) by substituting a hydrogen atom with a methylene CH₂ group. The radical stabilized by resonance and the unpaired electron is delocalized between the benzylic carbon atom and the benzene ring. In the junction setup, the amino groups are substituted at the 1,3-positions of the aromatic ring (usually referred to as the *meta* configuration in benzene) while the methylene group is substituted at the benzene 5-position, i.e., along the longer branch of the substituted ring. In this case, the SOMO displays its largest projection on the p_z LO of the benzylic carbon atom, with alternating nodes on the ring carbons, but negligible weight on the anchoring groups, thus suggesting a weak coupling to the electrodes. The benzyl resonant structures, the substituted molecule, and the projection of the SOMO onto the p_z LOs of the active space are shown in Figs. 2(d,e,f), respectively.

The comparison highlights a key difference: the pentadienyl SOMO has a sizable projection on the N-p_z LOs of the amino groups, whereas in benzyl it displays nodes. This distinction anticipates the drastically different transport properties of the two radical junctions.

B. Coulomb parameters in the LO basis

The partially screened cRPA Coulomb matrix projected onto the LO basis of the active space is shown in Figs. 3(a,b) for the pentadienyl and the benzyl radicals, respectively. We adopt the simplified notation $U_{ij} = \mathbf{U}_{A;ij}$. In both cases, the intra-orbital Coulomb interaction parameters are in the range of $U_{ii} \approx 4$ –5 eV and are slightly stronger for the atoms farther away from the metallic Au electrons, due to a weaker screening. Similar values of the Coulomb repulsion are found for the amino anchoring groups. However, as we shall discuss later in more detail, the C-p_z LOs are generally close to half-filling, where correlations are the strongest, whereas the N-p_z LOs are closer to being fully occupied, thus resulting in weaker correlations.

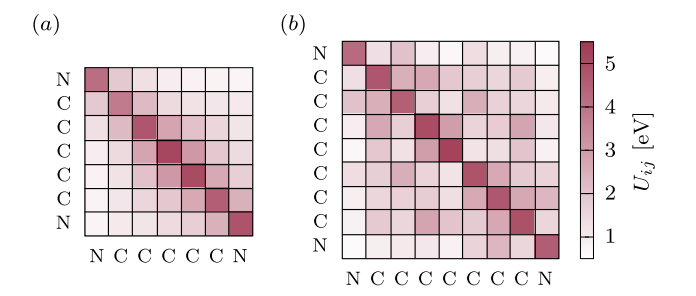


Figure 3. Partially screened Coulomb parameters $U_{ij} = \mathbf{U}_{A;ij}$ in the LO basis for (a) pentadienyl and the (b) benzyl radicals.

V. ELECTRON TRANSPORT

In this section, we present the electron transport properties of single-molecule junctions with pentadienyl and benzyl derivative bridges. We compare the predictions of DFT+NEGF with approaches that take into account many-body effects at a level of approximation beyond DFT, and show that the two radicals exhibit very different electronic and transport properties. In particular, we show that different treatments of the spin degree of freedom result in *qualitatively* different mechanisms for the splitting of the SOMO resonance. Which scenario applies in reality should be determined through experiments.

A. Pentadienyl

Within DFT, the transmission function displays a resonance close to the Fermi energy (denoted by E_F) corresponding to ballistic transport through the SOMO. The resonance is found at $\epsilon_{\rm SOMO}=70$ meV and has a width $\Gamma_{\rm SOMO}\approx 300$ meV, reflecting a significant hybridization of the SOMO with the states of the electrodes. The slight misalignment between the SOMO resonance and E_F , yields a conductance $G=5.7\times 10^{-1}~G_0$ in each spin channel, see Fig. 4(a). This scenario changes as the SOMO resonance is split due to the Coulomb repulsion. However, as we shall discuss below, depending on the splitting mechanism, we observe fundamentally different transport properties.

Symmetry-breaking. In the spin-unrestricted R-DMFT simulations, the spin-doublet degeneracy is lifted explicitly by applying a symmetry-breaking field, which is then removed during the self-consistent loop. The SOMO position displays a spin-dependent shift, with an occupied state (\psi-SOMO) in the majority-spin channel and an unoccupied state (\frac{\}-SUMO) in the minority-spin channel. Thus, the system realizes a magnetic insulator with a spin gap $\Delta_s \approx 1.0 \text{ eV}$ and a magnetic moment $\langle S_z \rangle \simeq 1/2$ due to the single unpaired electron. A corresponding resonance is found in each of the spin-resolved transmission functions, as shown in Fig. 4(a). The spin-dependent shift is approximately symmetric around the Fermi level. yielding a similar conductance in the two spin channels $G^{\downarrow} = 3.1 \times 10^{-2} G_0$ and $G^{\uparrow} = 1.1 \times 10^{-2} G_0$ and low spinfiltering efficiency. Probing the transmission $T = T^{\uparrow} + T^{\downarrow}$ without spin resolution would result in a pair of resonances, associated with a SOMO-SUMO splitting and a conductance $G = G^{\uparrow} + G^{\downarrow} = 4.2 \times 10^{-2} G_0$. Importantly, deep in the symmetry-broken phase, the manybody self-energy displays a weak energy dependence (see also Sec. VI) and similar results would be obtained by the static mean-field Hubbard [57] or DFT+U approaches. Breaking the spin symmetry is a common approach often used in the literature, and the spin-dependent shift of a transmission resonance [25, 43, 140] or antiresonance [59, 60], has been suggested as a suitable mechanism for the realization of organic spin filters.

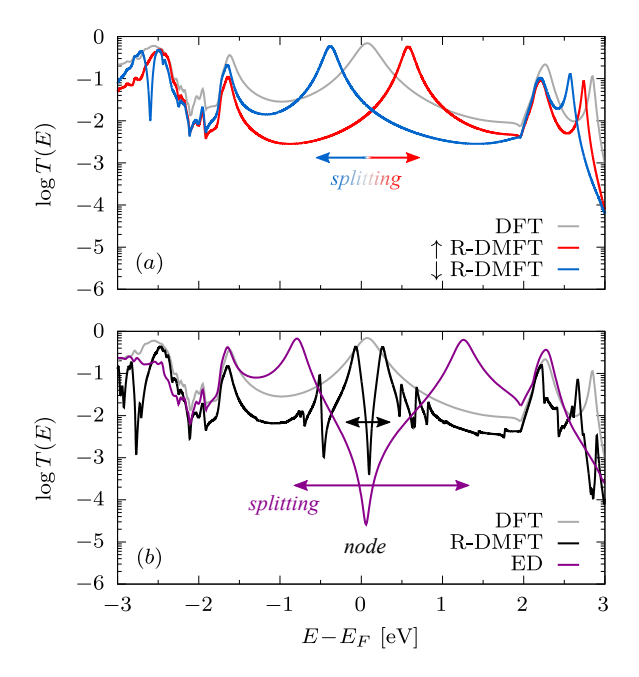


Figure 4. Electron transmission function through the pentadienyl radical junction. DFT predicts a SOMO resonance close to E_F . Taking into account the Coulomb repulsion beyond restricted DFT yields: (a) a splitting of the resonance into \downarrow -SOMO and \uparrow -SUMO due to spin-symmetry breaking; (b) a splitting of the resonance due to many-body effects (without spin symmetry breaking) revealing a transmission node close to the Fermi energy.

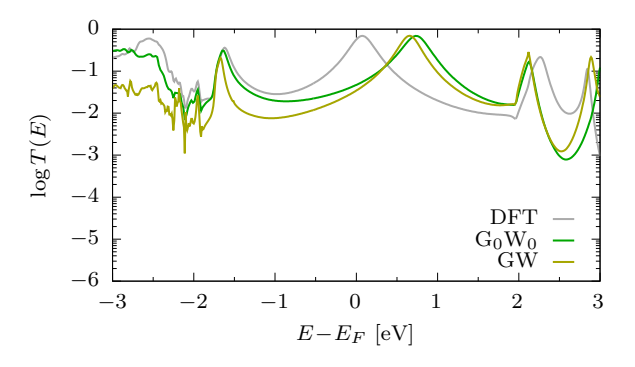


Figure 5. Electron transmission function through the pentadienyl radical junction. Both the G_0W_0 and the self-consistent GW approximations fail to predict the splitting of the SOMO feature, as described within ED and R-DMFT, cfr. Fig. 4.

Many-body splitting. The scenario is completely different within either spin-restricted R-DMFT or ED, in which many-body effects are accounted for without breaking the spin symmetry. In this case, we find that the SOMO transmission resonance is split in each spin channel, revealing an underlying transmission node that is absent in the symmetry-breaking solution, see Fig. 4(b). Hence, many-body calculations predict a strong suppression of the conductance, by several orders of magnitude, in stark contrast with the single-particle picture, where

electron transport is dominated by a nearly-resonant ballistic channel through the SOMO. Note that the splitting is substantially larger in ED than in R-DMFT, and considering that the antiresonance is not aligned with E_F , it also results in a much stronger suppression of the conductance $G = 1.2 \times 10^{-4} \ G_0$ (ED) versus $G = 7.4 \times 10^{-2} \ G_0$ (R-DMFT). This suggests that while the driving mechanism has a local nature, non-local correlation effects play an important quantitative role, as is expected in lowdimensional systems [56, 61]. Such a transmission node in the pentadienyl radical has been observed and analyzed within the framework of a single AIM [45]. Since linear π -conjugated molecules do not display any topological nodes, it has been suggested that this arises from destructive interference between different charged states of the molecule [45]. In Sec. VI, we discuss in detail the microscopic mechanism responsible for the splitting of the SOMO and for the transmission node, and show that they are intertwined.

Non-perturbative nature of the splitting Within ED and R-DMFT, the Coulomb repulsion is taken into account in a non-perturbative way. It is therefore interesting to compare these results to a perturbative approach, such as the GW approximation [141, 142], which has been extensively applied to molecules [143–148]. This raises the question of how reliably many-body perturbation theory can capture the physics of open-shell systems [149]. The GW approximation arises naturally within the context of Hedin equations by neglecting vertex corrections (see, e.g., [150]) and the GW self-energy is computed as a convolution of the Green's function and the screened Coulomb interaction. We compute the GW self-energy projected onto the A subspace

$$\Sigma_{GW}(z) = i\mathbf{G}_A(z)\mathbf{W}_A(z), \tag{30}$$

with the procedure described in [121]. The self-energy can be calculated either using the bare Green's function (G_0W_0) approximation) or by self-consistently dressing the Green's function with $\Sigma_{\rm GW}$. In Fig. 5 we show that neither the G_0W_0 nor the fully self-consistent GW approximation can induce a splitting of the SOMO resonance. Instead, both yield only a shift of the resonance above the Fermi energy, which in the junction setup, corresponds to a charge redistribution from the molecule to the electrodes, rather than a true oxidation of the radical.

Ultimately, we have shown a set of different mechanisms for the splitting of the SOMO. All result in a suppression of the conductance with respect to the single-particle DFT simulation, but exhibit very different transport properties. This suggests that focusing on the value of G/G_0 alone, one remains blind to the underlying microscopic mechanism. Importantly, our analysis demonstrates that the many-body techniques that we propose to investigate open-shell molecules are not only sufficient but also necessary to capture strong correlation effects, whereas common, yet less sophisticated, approaches such as GW or DFT+U fall short in describing certain electronic and transport properties of organic radicals.

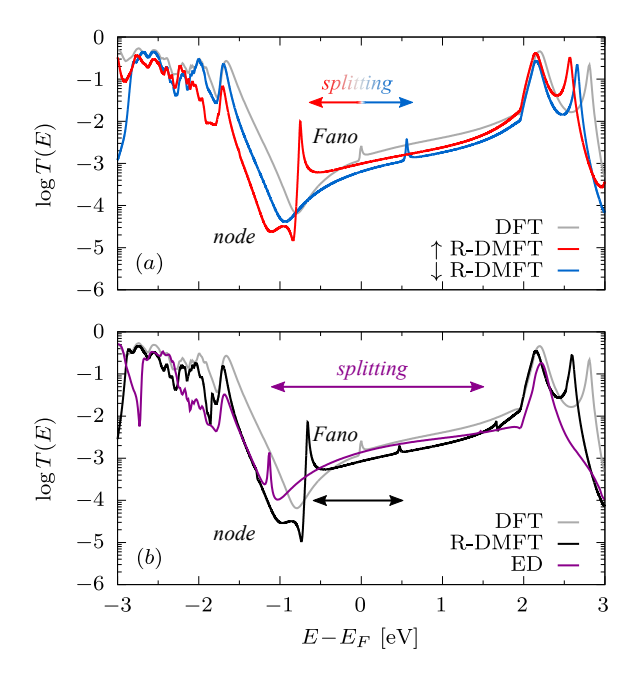


Figure 6. Electron transmission function through the benzyl radical junction. DFT predicts a SOMO resonance close to E_F . Taking into account the Coulomb repulsion beyond restricted DFT yields a spin-splitting of the Fano resonance of many-body origin (ED and restricted R-DMFT) or due to the spin-symmetry breaking (unrestricted R-DMFT). The QI node present at all levels of theory at ϵ_{QI} arises due to the meta-connection of the substituted benzene ring.

B. Benzyl

In single-molecule junctions with a benzene functional unit, there are a few possible configurations for the molecule bridging the electrodes, depending on the relative position of the substituted amino anchoring groups. We focus on the *meta* configuration, with amino groups at the 1,3-positions of the aromatic ring, which exhibits quantum interference (QI) effects which are particularly relevant in the context of molecular electronics.

Single-particle quantum interference. Within DFT, the transmission function displays two striking features which can be readily identified in Figs. 6(a,b): a narrow asymmetric Fano resonance at $\epsilon_{\rm Fano} < 10$ meV, close to E_F , and a wide antiresonance at $\epsilon_{\rm QI} \approx -0.8$ eV. Both features originate from QI effects. Clarifying the nature of the resonances and highlighting their differences is helpful to understand how electronic correlations affect the transport properties.

The antiresonance is the hallmark of destructive QI and it is well-established in the literature, from both the experimental [151–153] and theoretical [154–158] points of view. It is a common feature in molecular junctions with π -conjugated hydrocarbon bridges. It arises from the interference between MOs [158] and can be exploited for a wide range of applications [159] including chemical sensing [160, 161].

The resonance with a characteristic asymmetric Fano line shape arises from QI between a discrete state and a continuum background. [162, 163] Here, they correspond to the narrow SOMO resonance, which has nodes at the anchoring groups and is thus weakly coupled to the electrodes, and the MOs delocalized along the molecular backbone, with a strong overlap to the states of the Au electrodes [164]. Hence, the Fano resonance can be regarded as the transport signature of the SOMO. Due to the different shape of the SOMO resonance in the two radicals, i.e., Lorentzian or Breit-Wigner for pentadienyl and asymmetric Fano for benzyl, it is interesting to investigate the effect of the Coulomb repulsion and highlight the differences between the two cases.

Within the DFT simulations, the transmission function displays a narrow Fano resonance close to E_F . Due to the presence of the wider QI antiresonance, the transmission function is strongly asymmetric across the Fermi energy and the Fano shape is partially concealed.

Symmetry-breaking. The spin-unrestricted R-DMFT yields a pair of spin-split Fano resonances, as shown in Fig. 6(a). They originate by the QI interference between the \uparrow -SOMO and \downarrow -SUMO spin-orbitals with the other MOs. In the majority spin channel, $\epsilon_{\rm Fano}^{\uparrow} < 0$ falls within the energy region in which the transmission is suppressed by the antiresonance, and the asymmetric Fano profile is clearly observable. Its counterpart in the minority spin channel is found at $\epsilon_{\text{Fano}}^{\downarrow} > 0$, and is mostly concealed by the background transmission. Interestingly, the spin-symmetry breaking also induces spinresolved QI antiresonances, already observed in the literature [27, 59, 60, 165, 166] but the spin splitting $\epsilon_{\rm QI}^{\downarrow} - \epsilon_{\rm QI}^{\uparrow}$ is weaker than for the Fano resonance. This is because the spin imbalance $\langle S_z \rangle \simeq 1/2$ due to the unpaired electron is mostly localized on the p_z LO of the benzylic C atom, while the rest of the molecule is weakly magnetic. Similar results are observed in the literature, when electron-electron interactions are included at the static mean-field level within DFT+U and the spin symmetry is broken [43].

Many-body splitting. Again, performing many-body simulations without lifting the spin symmetry reveals another scenario, as shown in Fig. 6(b). The difference is twofold. We observe a splitting of the Fano resonance in both R-DMFT and ED (significantly larger for the latter), but no splitting is detected for the QI antiresonance, which is rather shifted away from E_F . This suggests that the microscopic mechanisms behind the splitting with and without spin-symmetry breaking are fundamentally different, because they distinguish between the two QI features. Moreover, in contrast to the case of pentadienyl, the splitting of the SOMO Fano resonance in benzyl does not result in a strong suppression of the transmission within the SOMO-SUMO gap. The two observations above are deeply connected and can be rationalized in terms of the spatial distribution of the SOMO. The GW results for benzyl are similar to those for pentadienyl, and justify analogous conclusions (not shown).

VI. MICROSCOPIC MECHANISM

A. Splitting of the SOMO

So far, we have seen that the Coulomb repulsion induces a splitting of the SOMO of the organic radicals. In order to gain a deeper understanding of the electronic mechanism behind the splitting, and how it affects the transport properties of the junction, it is useful to look at the retarded self-energy in the LO basis. We adopt the simplified notation $\Sigma_{ij} = \Sigma_{A;ij}$, for both Σ_A^{ED} and $\Sigma_A^{\sigma, R-DMFT}$ defined in Eqs. (13) and (20), respectively. The many-body effects encoded in the self-energy can be rationalized by interpreting the real part as an energydependent level shift, and the imaginary part as an effective electron-electron scattering rate. We argue that the mechanism discussed in the following is a generic feature of organic radicals with a single unpaired electron. Therefore, we discuss pentadienyl and benzyl radicals in parallel and highlight any differences whenever necessary.

In order to compare the different approximations, it is convenient to look at the trace of the self-energy matrix. Within spin-unrestricted R-DMFT, which is shown in Figs. 7(a,d), the real part of the self-energy is weakly energy-dependent around E_F , and determines a shift of the SOMO resonance in opposite directions for the two spin polarizations. The imaginary part is negligible (not shown) resulting in highly coherent SOMO and SUMO electronic excitations below and above E_F . Note that the ground state of spin-unrestricted R-DMFT is twofold degenerate, and it is invariant under a flip of all spins: $\{\sigma_i\} \to \{\bar{\sigma}_i\}$. This picture is qualitatively analogous to what one can expect also at the single-particle level, i.e., within DFT+U. Many-body effects are weak, and the dominant effect arises from the spin-symmetry breaking, as both radicals are magnetic insulators with a spin SOMO-SUMO gap.

The scenario is completely different within restricted R-DMFT and ED, as shown in Figs. 7(b,c,e,f). There, the self-energy is dominated by a single resonance and its energy dependence can be well described within a one-pole approximation (OPA)

$$\Sigma_{\text{OPA}}(E) = \frac{a^2}{E - E_F - \epsilon_{\text{res}} + i\gamma}.$$
 (31)

The OPA self-energy has a Lorentzian shape, where $\epsilon_{\rm res}$ and γ denote the resonant energy and the width of the resonance, whereas a controls the amplitude. In the simulations, the imaginary part of the self-energy plays the role of a giant electron-electron scattering rate and suppresses electronic excitations around $\epsilon_{\rm res} \simeq \epsilon_{\rm SOMO}$, while the real part redistributes the spectral above and below the resonance energy. This many-body mechanism, akin to the Mott metal-to-insulator transition as described within DMFT [96], is at the origin of the splitting of the SOMO resonance. Remarkably, this feature is completely absent in the GW self-energy, whose real part displays a

weak energy dependence, whereas the imaginary part is negligible close to the SOMO resonance (not shown) confirming the non-perturbative nature of the splitting.

In organic radicals, a hierarchy of emergent energy scales is realized: $\Gamma_{\text{SOMO}} \ll \Delta < \Delta_0 \lesssim U_{\text{screened}}$, where $\Delta_0 \sim \text{eV}$ denoted the HOMO-LUMO gap, controlled by the C-C π -bonds, and Δ is the SUMO-SOMO many-body splitting. Hence, the typical energy scale associated with the screened Coulomb repulsion U_{screened} significantly exceeds the width of the SOMO resonance ($\Gamma_{\rm SOMO} \sim 10$ -100 meV), which is controlled by the strength of the coupling to the electrodes. This scenario sets the electrons of the radicals considered here in the strongly correlated regime. Since these are typical energy scales for organic molecules, we argue that this mechanism is general for organic radicals with a single unpaired electron. In contrast, in closed-shell configurations, electronic correlations only result in a many-body renormalization of the single-particle gap [53–62]. Multi-radical molecules [167] and radical networks [22], are expected to display different electronic and transport properties due to effective interactions between the unpaired electrons [11, 20, 47, 48].

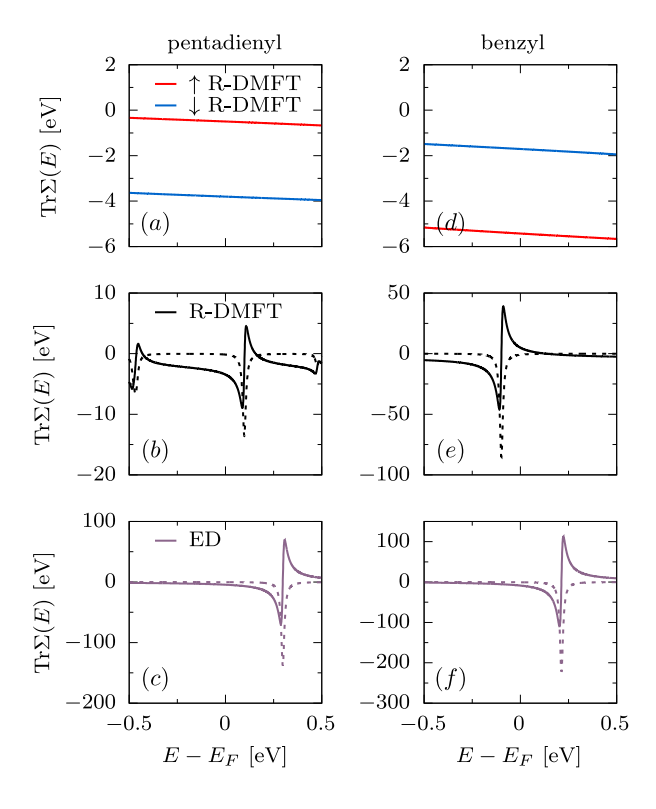


Figure 7. Trace of the retarded self-energy $\text{Tr}[\Sigma(E)]$ in the LO basis for the pentadienyl (a, b, c) and benzyl (d, e, f) radicals (the real and imaginary parts are denoted by solid and dashed lines, respectively). Within spin-unrestricted R-DMFT (a, d) the self-energy displays a weakly energy-dependent real part, which is different in each spin sector, while the imaginary part is negligible (not shown). Within both R-DMFT (b, e) and ED (c, f) the self-energy is dominated by a single resonance.

B. Spatial structure of the electronic correlations

So far, R-DMFT and ED seem to qualitatively describe the same many-body mechanism for the splitting of the SOMO. However, besides the trace of the self-energy, it is interesting to visualize the whole self-energy matrix. As discussed in Sec. IIC, within ED all elements $\Sigma_{ij} \neq 0$, whereas within R-DMFT $\Sigma_{ij} \propto \delta_{ij}$. Remarkably, all elements of the self-energy (regardless of the approximation) are well described by the OPA with the same resonant energy ϵ_r , as shown in Figs. 8(a, e). The off-diagonal elements can have either sign, but causality requires Im $\Sigma_{ii} < 0$. It is easier to have a comprehensive look at the self-energy by plotting the matrix $\Sigma_{ij}(\epsilon_r)$, as shown in Figs. 8(c, d, g, h). Indeed, looking at the ED self-energy matrix, clear patterns emerge. Along the diagonal, some elements Σ_{ii} are significantly larger than the others (note the logarithmic scale), and this asymmetry is mirrored by the off-diagonal elements. Upon close inspection, we can associate them with the p_z LOs with the largest SOMO projection, thus confirming that the strongest many-body effects correlate with the spatial distribution of the SOMO. Within R-DMFT, we find an analogous pattern along the diagonal, as indicated by the insets molecules.

Despite its approximations (local Coulomb interaction, local correlations), restricted R-DMFT seems to tell qualitatively the same story as the full ED simulations. This advocates for a substantially local character of the microscopic mechanism, that can describe both the splitting of the SOMO and its consequences on electron transport, whereas non-local effects only result in a quantitative renormalization of the SOMO-SUMO splitting.

C. Implications for electron transport: insights from a minimal model

The many-body mechanism behind the splitting of the SOMO is common to both the pentadienyl and benzyl radicals. However, its consequences on electron transport are dramatically different. To understand why, we combine the insights from DFT and the knowledge of the spatial and energy structure of the self-energy as follows.

In pentadienyl, the SOMO is delocalized throughout the molecular backbone, and its large projection on the p_z LOs of the amino anchoring groups, see Fig. 2(a), ensures a substantial overlap with the states in the metallic electrodes and establishes a transmission channel across the junction through the SOMO. However, the pole of the self-energy results in a zero of the Green's function. which hinders electron transport at that energy and is at the origin of the transmission node [59, 60]. In contrast, in the benzyl radical, the SOMO has negligible projection on the amino anchoring groups, see Fig.2(d), and transport is dominated by transmission channels involving the frontier MOs. Therefore, the splitting of the Fano resonance weakly affects those channels and does not hinder

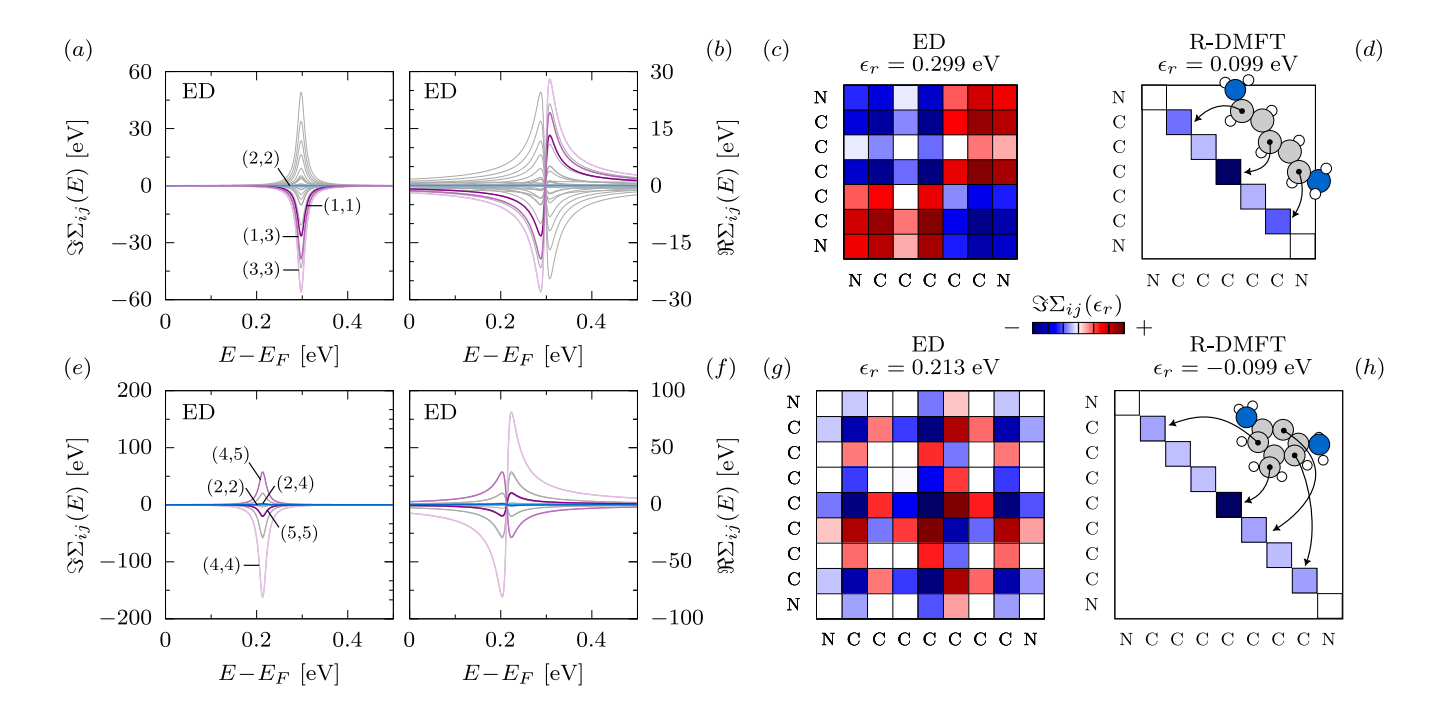


Figure 8. Component of the ED self-energy $\Sigma_{ij}(E)$ and its matrix representation at the resonant energy Im $\Sigma_{ij}(\epsilon_{\rm res})$ in the LO basis for the pentadienyl (a,b,c,d) and benzyl (e,f,g,h) radicals. Each component of the self-energy (grey lines) is dominated by a single pole (a,b,e,f) at a resonant energy ϵ_r . Selected components (i,j) are highlighted (color lines) and are labeled according to their index in the matrix, starting with Σ_{00} for the left N-p_z LO. The matrix structure of the self-energy reflects the spatial distribution of the SOMO, i.e., the largest local (Σ_{ii}) and non-local $(\Sigma_{ij\neq i})$ self-energy contributions are found for the LOs with the largest projections to the SOMO (denoted by arrows, see also Fig. 2). Within R-DMFT (d,h) the self-energy is diagonal in the LO indices $\Sigma_{ij} \propto \delta_{ij}$ and displays the same pattern.

off-resonant transmission of electrons across the junction.

The above picture can be reproduced within a minimal tight-binding (TB) model, which is schematically represented in Fig. 9(a). Let us consider three AOs (ℓ, c, r) that can be interpreted as the C-p_z orbitals, whereas the anchoring groups are absorbed in an effective description of the reservoirs. The Hamiltonian in such a basis reads

$$\mathbf{H} = \begin{pmatrix} \epsilon_{\ell} & t & t' \\ t & \epsilon_{c} & t \\ t' & t & \epsilon_{r} \end{pmatrix} . \tag{32}$$

The hybridization to the electrodes is mediated by the external orbitals (ℓ, r) which bond to the anchoring groups, and for the sake of this discussion, it is assumed to be energy-independent:

$$\mathbf{\Gamma}_L = \begin{pmatrix} \Gamma & 0 & 0 \\ 0 & 0 & 0 \\ 0 & 0 & 0 \end{pmatrix}, \ \mathbf{\Gamma}_R = \begin{pmatrix} 0 & 0 & 0 \\ 0 & 0 & 0 \\ 0 & 0 & \Gamma \end{pmatrix}. \tag{33}$$

The Hamiltonian of the isolated system can be diagonalized to obtain the eigenvalues $\epsilon_{\rm HOMO}$, $\epsilon_{\rm SOMO}$, and $\epsilon_{\rm LUMO}$. The Green's function of the device is given by

$$\mathbf{G}_{D}(z) = \left[z - \mathbf{H} + i\mathbf{\Gamma}_{L}/2 + i\mathbf{\Gamma}_{R}/2 - \mathbf{\Sigma}_{D}(z)\right]^{-1} \quad (34)$$

and is *dressed* with the retarded self-energy of the device $\Sigma_D(z)$. To pinpoint the microscopic mechanism behind

the many-body splitting of the SOMO resonance, we employ an OPA self-energy of the form

$$\Sigma_D(z) = \begin{pmatrix} 0 & 0 & 0 \\ 0 & \Sigma_{\text{OPA}}(z) & 0 \\ 0 & 0 & 0 \end{pmatrix}$$
 (35)

with

$$\Sigma_{\rm OPA}(z) = \frac{a^2}{z - \epsilon_{\rm res}},\tag{36}$$

where $z=E-E_F+i\gamma$, with a controlling the weight of the self-energy, and a self-energy pole located at the position of the SOMO resonance $\epsilon_{\rm res} \simeq \epsilon_{\rm SOMO}$. The OPA self-energy resembles the form of the self-energy obtained from the ab-initio+ many-body simulations, for which the largest contribution is the local element of the radical C atom; see Figs. 8(a-e) for a comparison.

Within such a three-orbital model, the Landauer transmission in Eq. (28) reduces to

$$T(E) = \Gamma^2 |G_{\ell r}(E)|^2,$$
 (37)

where $G_{\ell r} = \mathbf{G}_{D;\ell r}$ is the only element of the Green's function that survives the trace in the Landauer formula, given the form of the hybridization matrices Γ_L and Γ_R , and therefore describes the only transmission channel across the junction [168].

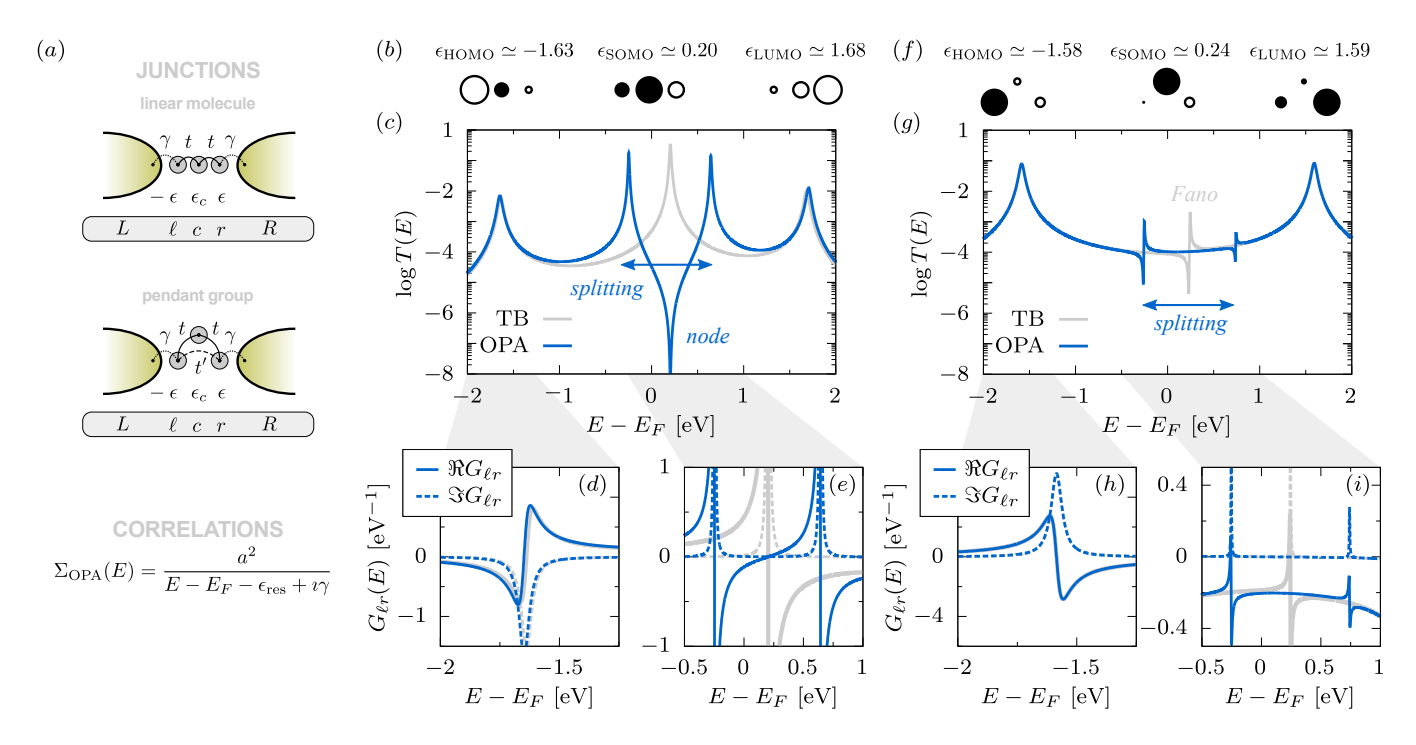


Figure 9. (a) Schematic representation of the two junction topology described by the three-orbital TB model with its parameter, and form of the OPA self-energy. (b,f) Weight distribution and eigenvalues of the TB MOs, in units of [eV]. Each MO is represented with circles centered at the position of the AOs, the circle size reflects the weight of the MO projection on the AOs, and the color (black/white) indicates the sign of the coefficient. (c,g) The transmission function obtained without (grey lines) and with (blue lines) the OPA self-energy. The OPA approximation captures all qualitative features of the ab-initio + many-body simulations. (d,e,h,i) The Green's function $G_{\ell r}$ is shown for specific energy ranges, which are relevant to explaining the spectral features associated with the HOMOs (d,h) and the SOMOs (e,i), as discussed in the text. Model parameters, in units of [eV]: $\epsilon = 1.5$, $\epsilon_c = 0.25$, a = 0.5, $\Gamma = 0.05$, $\gamma = 0.003$, common to both scenarios, linear molecules are represented by choosing t = 0.5, t' = 0 (b,c,d,e) whereas molecules with a pendant group are represented by choosing t = 0.1, t' = 0.5 (f,g,h,i).

For simplicity, one can fix $-\epsilon_{\ell} = \epsilon_r = \epsilon$, and $\epsilon_c \ll \epsilon$, together with a, Γ , and η , and choose the parameters t and t' to describe two scenarios, which are representative of the pentadienyl and benzyl radicals. The results are presented in Fig. 9 and discussed below.

The physics of the pentadienyl radical (or in general, a linear conjugated molecule with an odd number of C atoms) can be reproduced by choosing $t \lesssim \epsilon$ and t' = 0. Hence, electron transport occurs via tunneling processes between adjacent atoms, resembling through bond couplings between the corresponding AOs with amplitude t. The corresponding SOMO is fairly delocalized along the molecular backbone, with the highest projection of the central AO, cfr. Fig. 2(b) and Fig. 9(b). The TB transmission function in Fig. 9(c) displays a SOMO resonance that is split by including the OPA self-energy, thus revealing a transmission node within the SOMO-SUMO gap. The origin of the transmission node is ascribed to a zero of the Green's function at the SOMO energy $G_{\ell r}(E \simeq \epsilon_{\rm SOMO}) \approx 0$ [59, 60, 169], as demonstrated in Fig. 9(e).

Instead, with the choice of parameters $t \ll t' \lesssim \epsilon$, one can describe the physics of the benzyl radical, characterized by an orbital c, which is weakly coupled to the $\ell-r$ molecular backbone. The corresponding SOMO is fairly

localized on the orbital playing the role of the pendant group, with little weight on the orbitals connected to the reservoirs, cfr. Fig. 2(d) and Fig. 9(f). The transmission function in Fig. 9(g) displays a sharp Fano resonance that is split by the OPA self-energy. In contrast to the previous case, $G_{\ell r}$ does not have a zero within the SOMO-SUMO gap, and transport is dominated by a transmission channel along the molecular backbone, corresponding to the direct ℓ -r hopping process with amplitude t'. Finally, note that in both scenarios above, many-body effects are negligible for the HOMO and LUMO resonances (corresponding to orbitals that are either completely filled or empty) irrespective of whether the "correlated" c orbital has a sizable hybridization with ℓ and r, as can be inferred comparing Figs. 9(d,h).

Such a minimal model can reproduce all fundamental features for both radical junctions discussed in this work just by changing the parameters of the single-particle Hamiltonian to represent one or the other molecule. At the same time, it provides a simple and direct interpretation of the numerical simulations.

The splitting mechanism can be better understood by further reducing the minimal model to a single level at ϵ_c renormalized by an OPA self-energy, resonant at $\epsilon_{\rm res}$.

The corresponding Green's function reads

$$G(\omega) = \frac{1}{\omega - \epsilon_c - \Sigma_{\text{OPA}}(\omega)},$$
 (38)

with $\Sigma_{\text{OPA}}(\omega)$ given by Eq. (31). It can be shown that such a Green's function can be brought into a sum of two simple poles

$$G(\omega) = \left[\frac{b_{-}}{\omega - \omega_{-} + i\eta_{-}} + \frac{b_{+}}{\omega - \omega_{+} + i\eta_{+}} \right], \quad (39)$$

where the poles' positions ω_{\pm} , residues b_{\pm} , and damping factors $\eta_{\pm} > 0$ can be calculated exactly (see Appendix A). In the *strong coupling* limit $a/\gamma \gg 1$ the splitting between the poles $\omega_{+} - \omega_{-} \approx 2a$ and the damping $\eta_{\pm} \approx \gamma/2$, so that the two resonances are spectroscopically resolved.

Importantly, the residues b_{\pm} are in general *complex*, and the Green's function does not reduce to the sum of two independent resonances. As a consequence, the transmission function $T(\omega) \propto |G(\omega)|^2$, with

$$|G(\omega)|^{2} = \frac{|b_{+}|^{2}}{|\omega - \omega_{+} + i\eta_{+}|^{2}} + \frac{|b_{-}|^{2}}{|\omega - \omega_{-} + i\eta_{-}|^{2}}$$
(40)
+
$$2 \operatorname{Re} \left[\frac{b_{+}b_{-}^{*}}{(\omega - \omega_{+} + i\eta_{+})(\omega - \omega_{-} - i\eta_{-})} \right].$$
(41)

The first two contributions correspond to tunneling probabilities through the split SUMO and SOMO resonances at $\omega_{\pm} \approx (\epsilon_c + \epsilon_{\rm res})/2 \pm a$, whereas the mixed contribution is responsible for QI. In the specific case we considered, the mixed contribution is negative for $\omega_{-} \lesssim \omega \lesssim \omega_{+}$ and suppresses the transmission probability at energies between the resonances, resulting in a QI node at $\omega = \epsilon_{\rm res}$ (resonant condition for $\Sigma_{\rm OPA}$). When $\epsilon_c = \epsilon_{\rm res}$, the splitting is symmetric around the QI node.

VII. $I - V_b$ CHARACTERISTICS

So far, we have demonstrated that different microscopic mechanisms underlying the splitting of the SOMO resonance (i.e., the many-body or magnetic splitting of the SOMO resonance), a Fermi energy alignment, or the oxidation of the radical, result in different distinctive features in the electron transmission function. A natural question is whether it is possible to discriminate between these scenarios. Experiments have direct access to the current-bias $I - V_b$ characteristics, but a possible strategy to probe the transmission function is to consider the differential conductance in the low-bias regime, where $dI/dV_b(V_b)$ resembles T(E). It has been shown [170] that in the presence of an antiresonance at ω_{QI} a "v-shaped" differential conductance is measured at low bias, whereas a "u-shaped" differential conductance typically suggests constructive QI instead. However, the profile of the differential conductance is sensitive to the relative alignment of ω_{OI} and the Fermi energy, and is not entirely conclusive [170].

An alternative fingerprint of destructive QI is a strongly non-linear $I-V_b$ characteristics in the non-resonant transport regime [169, 171]. In Fig. 10, we show that, in the case of pentadienyl, a QI node in the transmission function corresponds to a strong non-linearity $I-V_b$ curve that is already dominant before the onset of the resonant transport regime. The underlying argument is simple. The current in terms of the transmission function is given by

$$I = \frac{e}{h} \int_{-\infty}^{\infty} d\omega T(\omega) \left[f_L(\omega) - f_R(\omega) \right], \qquad (42)$$

where $f_L(\omega) = f(\omega + eV_b/2)$ and $f_R(\omega) = f(\omega - eV_b/2)$, are the Fermi-Dirac distributions of the left and right electrodes, respectively, with $f(\omega) = (1 + e^{-\omega/k_BT})^{-1}$. Near equilibrium, i.e., $T(\omega, eV_b) \approx T(\omega)$, off-resonance, and in the limit $k_BT \ll eV_b$, two scenarios are possible:

- (i) in the absence of a QI node, the transmission function is nearly constant $T(\omega \approx 0) \approx \tau_0$, yielding a linear characteristics, $I(V_b) \propto V_b$;
- (ii) in the presence of a QI node at ω_{QI} , it can be shown that $T(\omega \to \omega_{\text{QI}}) \approx \tau_0 + \tau_2 (\omega \omega_{\text{QI}})^2$, thus yielding both a linear and a cubic contribution upon integration: $I(V_b) \approx \alpha_1 V_b + \alpha_3 V_b^3$.

The behavior of the transmission function follows from the analysis of the real-space retarded Green's function, for which the real part linearly change sign across the QI node, $\operatorname{Re} G_{\ell r}(\omega \to \omega_{\rm QI}) \propto \omega - \omega_{\rm QI}$ [59, 60, 169].

It is useful to analyze the coefficients and, in particular, the effective curvature $r = (\alpha_3/\alpha_1)(eV_b)^2$ given by the ratio of the linear and cubic terms (note that the quadratic term is zero because of integrating an odd function over a symmetric bias window). Considering the minimal model in the regime in which the splitting is spectroscopically resolved $(a\gamma \gg 1)$ one typically expects a linear regime (r < 1) at sufficiently low bias, and an extended non-linear regime (r > 1) far from resonant tunneling, which, in terms of the parameter of our model, is roughly equivalent to $eV_b/2 \lesssim a - |\omega_{\rm QI}|$. Close to resonant transport, additional non-linear terms arise because the transmission has non-negligible contributions from the resonance. Therefore, far from resonant tunneling, a strong non-linear $I-V_b$ characteristic can be interpreted as a fingerprint of destructive QI. These considerations provide a clear interpretation of the numerical results.

In Fig. 10 we compare the conductance G/G_0 and the $I-V_b$ characteristics obtained for both radical junctions at each level of theory. For pentadienyl, see Fig. 10(a), the first observation is that the conductance alone is not sufficient to discriminate between the different scenarios. Apart from the DFT+NEGF transport simulations, all simulations that include many-body effects yield a conductance that is incompatible with nearly-resonant transport. In particular, ED yields the lowest conductance because of the wide gap and deep QI node. In the spin-restricted R-DMFT, the conductance is deceptively

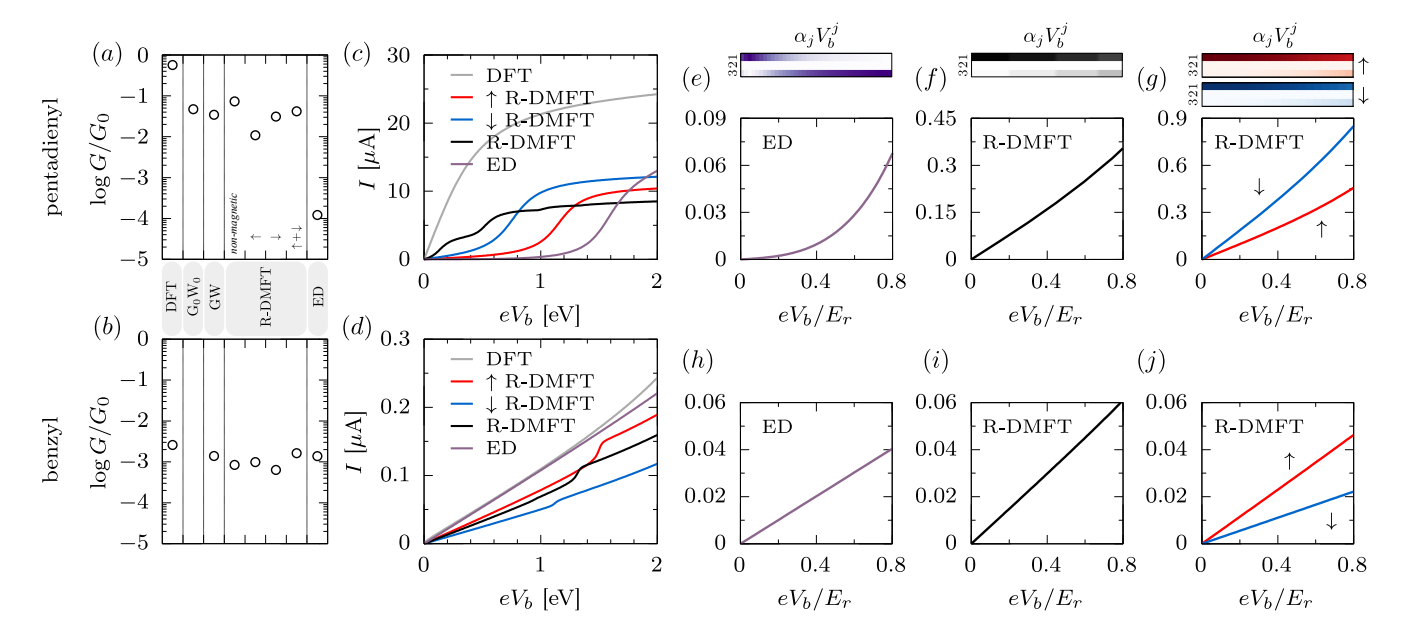


Figure 10. (a, b) Comparison of the electron conductances G/G_0 and (c, d) current-voltage $(I-V_b)$ characteristics obtained at different levels of theory, for both the pentadienyl and benzyl molecular junctions. (c,d) Comparison of the $I-V_b$ curves from the different theoretical approaches. (e,f,g) $I-V_b$ characteristics in the low-energy bias window in pentadienyl, measured with respect to the lowest transmission resonance at energy $|E_r|$. For each value of V_b we perform a numerical fit of the curve with $I(V_b) = \sum_{j=1}^3 \alpha_j V_b^j$, and the colorbars above each panel show the relative weight of the j-th term. Note that the quadratic term is zero because of integrating an odd function over a symmetric bias window. Non-linear contributions are significant in ED but weaker in R-DMFT (see the text for a detailed discussion). (h,i,j) $I-V_b$ characteristics in the low-energy bias window in benzyl, measured with respect to the lowest transmission resonance at energy $|E_r|$. The narrow Fano resonance does not result in an appreciable deviation from Ohmic behavior.

higher than in the spin-unrestricted case $(G > G^{\downarrow} > G^{\uparrow})$ because of the narrow SOMO-SUMO splitting. This is also reflected in the $I - V_b$ characteristics. In Fig. 10(c) we show the current as a function of bias obtained at all levels of theory. The rapid increase of the DFT current at low bias is consistent with the nearly-resonant transport regime.

In Figs. 10(e, f, g) instead, we highlight the different behavior of the many-body simulations by rescaling the bias to E_r , corresponding to the distance of the closest transport resonance from the Fermi energy. ED displays a low current and a strongly non-linear characteristic, with the cubic term $\alpha_3 V^{\bar{3}}$ dominant already at $eV_b/E_r \gtrsim 0.2$. This is the hallmark of the QI node within the wide SOMO-SUMO gap. In contrast, R-DMFT displays a nearly linear characteristic. The rise of a nonlinear term at $eV/E_r \gtrsim 0.4$ can be ascribed to the QI node, but it is weak because (i) the SOMO-SUMO splitting is narrow and (ii) the Fermi level lies very close to one of the split-SOMO resonances. This is the worst-case scenario, in which the QI node is present but very difficult to identify from the non-linear characteristic. In the spin-unrestricted R-DMFT the QI node is absent, a weak non-linear term appears in both spin channels only at $eV_b/E_r \gtrsim 0.8$, and it is completely associated with the vicinity to the transport resonance at E_r .

For benzyl, we obtain conductance values $G \simeq 10^{-3} G_0$

at all levels of theory, see Fig. 10(b) and linear $I-V_b$ characteristic up to $eV_b/E_r\lesssim 1$, see Figs. 10(d, h, i, j). This is explained considering that the narrow Fano resonance(s) do not generate a contribution to the current large enough to be detected over the linear background within the HOMO-LUMO gap. So, in this case, the $I-V_b$ characteristic is not useful in identifying the SOMO splitting.

VIII. CONCLUSIONS

In this work, we have unraveled the emergence of strongly correlated electron physics in radical molecules with a single unpaired electron. We identify the splitting of the SOMO resonance as a hallmark of many-body effects, with observable consequences in the electron transport in a two-terminal junction setup. We argue that this phenomenon can explain puzzling evidence such as the low conductance observed in transport measurements.

Specifically, we performed thorough numerical simulations combining state-of-the-art *ab-initio* and many-body techniques. Our framework can describe the complexity of a realistic chemical environment as well as electronic correlation effects beyond the single-particle picture, and it is specifically tailored to address the electron transport properties of quantum junctions. By considering

a linear and a cyclic radical species, we obtain a general understanding of the role of many-body effects in molecular radicals with a single unpaired electron, and their dramatic consequences on electron transport. We establish the microscopic mechanism behind the splitting of the SOMO resonance and discover a clear link between the structure of the electronic self-energy and the spatial distribution of the SOMO. We further demonstrate this through a minimal model that reproduces the key phenomenological features of the electron transmission. Moreover, we demonstrate that a non-perturbative treatment of the Coulomb repulsion is paramount to describe the splitting of the SOMO resonance, and alternative common approaches, such as many-body perturbation theory or static mean-field (which breaks the spin symmetry) fail to reproduce it, resulting in qualitatively different features and suggesting different interpretations of the underlying physics.

All approaches that treat the Coulomb repulsion beyond DFT exhibit a suppression of the conductance, which is incompatible with nearly-resonant transport through an open channel. Beyond the zero-bias conductance, the $I-V_b$ characteristics offer an additional perspective on the role of many-body effects. In the pentadienyl junction, the correlation-induced splitting of the SOMO gives rise to a spectroscopically resolved transmission node, leading to strongly nonlinear $I - V_b$ behavior at low bias. This provides an experimentally accessible signature of strong correlations by measuring destructive quantum interference that can arise neither in the single-particle picture nor in mean-field or perturbative approaches. In contrast, for the benzyl junction, the $I-V_b$ curves are qualitatively identical across DFT and many-body approaches, reflecting the weak coupling of the SOMO to the electrodes. Many-body effects in benzyl remain spectroscopically silent in transport, and the narrow Fano resonances are hardly observable in the $I-V_b$ response. This underscores the importance of molecular orbital alignment and spatial distribution of the MOs in determining whether correlations manifest in measurable transport quantities.

Finally, we note that the present work neglects vertex corrections in the transmission function, which take into account inelastic electron-electron scattering processes. In open-shell molecular junctions, such as those investigated here, these corrections are expected to be sizable, or even the dominant contribution [168], in the resonant tunneling regime. Their inclusion is anticipated to introduce additional broadening and asymmetric reshaping of the transmission and interference features, while preserving the overall qualitative behavior discussed in this work. A quantitative evaluation of vertex corrections will be the subject of future investigations.

Overall, our study establishes a framework to understand how strong electronic correlations manifest in the transport properties of organic radicals. In particular, it highlights that different treatments of the spin degree of freedom result in qualitatively different transport prop-

erties, calling for experiments to discriminate between the different scenarios. Thus, our work paves the path toward a deeper and more comprehensive understanding of strongly correlated electron physics of organic radicals.

ACKNOWLEDGEMENTS

We thank J. M. Tomczak for valuable discussions and constructive feedback on the manuscript, This research is supported by the Austrian Science Fund (FWF) through project P 31631, the HUN-REN Hungarian Research Network through the Supported Research Groups Programme, HUN-REN-BME-BCE Quantum Technology Research Group (TKCS-2024/34). and the NCCR MARVEL funded by the Swiss National Science Foundation grant 51NF40-205602. Computational support from the Swiss Supercomputing Center (CSCS) under project ID s1119 is gratefully acknowledged.

Appendix A: Two-poles decomposition

Let us show how the Green's function

$$G(\omega) = \frac{1}{\omega - \epsilon_0 - \Sigma_{\text{OPA}}} \tag{A1}$$

with the one-pole approximation (OPA) self-energy

$$\Sigma_{\text{OPA}} = \frac{a^2}{\omega - \epsilon_{\text{res}} + i\gamma}.$$
 (A2)

can be brought into the sum of two simple poles

$$G(\omega) = \left[\frac{b_{-}}{\omega - \omega_{-} + \imath \eta_{-}} + \frac{b_{+}}{\omega - \omega_{+} + \imath \eta_{+}} \right], \quad (A3)$$

where the poles' positions ω_{\pm} , residues b_{\pm} , and damping factors $\eta_{\pm} > 0$.

Let us define $x = \omega - \epsilon_0$ and $\delta = \epsilon_0 - \epsilon_{res}$. Then

$$G(x) = \frac{1}{x - \frac{a^2}{x + \delta + i\gamma}} = \frac{x + \delta + i\gamma}{x^2 + (\delta + i\gamma)x - a^2}$$
(A4)

takes the form G(x) = P(x)/Q(x) and the poles are the roots of the quadratic denominator

$$x^{2} + (\delta + i\gamma)x - a^{2} = 0.$$
 (A5)

Let us further define

$$\Delta \equiv \sqrt{4a^2 + (\delta + \gamma)^2} \tag{A6}$$

then the two roots given by

$$x_{\pm} = \frac{-(\delta + i\gamma) \pm \Delta}{2}.$$
 (A7)

The residues are given by

$$b_{+} = \frac{P(x_{+})}{x_{+} - x_{-}}, \qquad b_{-} = \frac{P(x_{-})}{x_{-} - x_{+}}$$
 (A8)

with $P(x) = x + \delta + i\gamma$ and $x_{+} - x_{-} = \Delta$, we obtain compact forms

$$b_{+} = \frac{x_{+} + i\gamma}{\Lambda}, \qquad b_{-} = -\frac{x_{-} + i\gamma}{\Lambda}. \tag{A9}$$

Equivalently, substituting the expression found for x_{\pm}

$$b_{+} = \frac{1}{2} + \frac{\delta + i\gamma}{2\Delta}, \qquad b_{-} = \frac{1}{2} - \frac{\delta + i\gamma}{2\Delta}.$$
 (A10)

and one can verify that $b_+ + b_- = 1$, which is consistent with the asymptotic behavior of the Green's function $G(\omega) \sim 1/(\omega - \epsilon_0)$ for $\omega \to \infty$.

- Z. Chen, Y. Li, and F. Huang, Chem 7, 288 (2021), URL https://doi.org/10.1016/j.chempr.2020.09.024.
- [2] L. Li, C. R. Prindle, W. Shi, C. Nuckolls, and L. Venkataraman, Journal of the American Chemical Society 145, 18182–18204 (2023), ISSN 1520-5126, URL http://dx.doi.org/10.1021/jacs.3c04487.
- [3] C. Shu, Z. Yang, and A. Rajca, Chemical Reviews 123, 11954–12003 (2023), ISSN 1520-6890, URL http://dx. doi.org/10.1021/acs.chemrev.3c00406.
- [4] F. Bejarano, I. J. Olavarria-Contreras, A. Droghetti, I. Rungger, A. Rudnev, D. Gutiérrez, M. Mas-Torrent, J. Veciana, H. S. J. van der Zant, C. Rovira, et al., Journal of the American Chemical Society 140, 1691 (2018), URL https://doi.org/10.1021/jacs.7b10019.
- [5] J. Hurtado-Gallego, S. Sangtarash, R. Davidson, L. Rincón-García, A. Daaoub, G. Rubio-Bollinger, C. J. Lambert, V. S. Oganesyan, M. R. Bryce, N. Agraït, et al., Nano Letters 22, 948-953 (2022), ISSN 1530-6992, URL http://dx.doi.org/10.1021/ acs.nanolett.1c03698.
- [6] G. Mitra, J. Zheng, K. Schaefer, M. Deffner, J. Z. Low, L. M. Campos, C. Herrmann, T. A. Costi, and E. Scheer, Chem p. 102500 (2025), ISSN 2451-9294, URL http://dx.doi.org/10.1016/j.chempr. 2025.102500.
- [7] J. Liu, X. Zhao, Q. Al-Galiby, X. Huang, J. Zheng, R. Li, C. Huang, Y. Yang, J. Shi, D. Z. Manrique, et al., Angewandte Chemie International Edition 56, 13061 (2017), URL https://doi.org/10.1002/anie. 201707710.
- [8] E. Pyurbeeva, C. Hsu, D. Vogel, C. Wegeberg, M. Mayor, H. van der Zant, J. A. Mol, and P. Gehring, Nano Letters 21, 9715-9719 (2021), ISSN 1530-6992, URL http://dx.doi.org/10.1021/ acs.nanolett.1c03591.
- [9] S. Naghibi, S. Sangtarash, V. J. Kumar, J. Wu, M. M. Judd, X. Qiao, E. Gorenskaia, S. J. Higgins, N. Cox, R. J. Nichols, et al., Angewandte Chemie International Edition 61 (2022), ISSN 1521-3773, URL http://dx.doi.org/10.1002/anie.202116985.
- [10] L. L. Patera, S. Sokolov, J. Z. Low, L. M. Campos, L. Venkataraman, and J. Repp, Angewandte Chemie International Edition 58, 11063 (2019), URL https://doi.org/10.1002/anie.201904851.
- [11] Y. Zheng, C. Li, C. Xu, D. Beyer, X. Yue, Y. Zhao, G. Wang, D. Guan, Y. Li, H. Zheng, et al., Nature Communications 11 (2020), URL https://doi.org/ 10.1038/s41467-020-19834-2.
- [12] R. Hayakawa, M. A. Karimi, J. Wolf, T. Huhn, M. S. Zöllner, C. Herrmann, and E. Scheer, Nano Letters

- 16, 4960 (2016), URL https://doi.org/10.1021/acs.nanolett.6b01595.
- [13] J. Liu, H. Isshiki, K. Katoh, T. Morita, K. B. Brian, M. Yamashita, and T. Komeda, Journal of the American Chemical Society 135, 651 (2012), URL https://doi. org/10.1021/ja303510g.
- [14] Y. hui Zhang, S. Kahle, T. Herden, C. Stroh, M. Mayor, U. Schlickum, M. Ternes, P. Wahl, and K. Kern, Nature Communications 4 (2013), URL https://doi.org/10. 1038/ncomms3110.
- [15] S. Zhang, M. Pink, T. Junghoefer, W. Zhao, S.-N. Hsu, S. Rajca, A. Calzolari, B. W. Boudouris, M. B. Casu, and A. Rajca, Journal of the American Chemical Society 144, 6059-6070 (2022), ISSN 1520-5126, URL http://dx.doi.org/10.1021/jacs.2c01141.
- [16] Y. Hou, H. Chen, W. Lian, H. Li, X. Hu, and X. Liu, Advanced Functional Materials 33 (2023), ISSN 1616-3028, URL http://dx.doi.org/10.1002/adfm.202306056.
- [17] H. Zhang, L. Chen, X. Liu, F. Sun, M. Zhang, S. M. Quintero, Q. Zhan, S. Jiang, J. Li, D. Wang, et al., Science Advances 10 (2024), ISSN 2375-2548, URL http://dx.doi.org/10.1126/sciadv.adp7307.
- [18] T. Bras, C. Hsu, T. Y. Baum, D. Vogel, M. Mayor, and H. S. J. van der Zant, The Journal of Physical Chemistry C 129, 3152-3157 (2025), ISSN 1932-7455, URL http://dx.doi.org/10.1021/acs.jpcc.4c05860.
- [19] J. Z. Low, G. Kladnik, L. L. Patera, S. Sokolov, G. Lovat, E. Kumarasamy, J. Repp, L. M. Campos, D. Cvetko, A. Morgante, et al., Nano Letters 19, 2543 (2019), URL https://doi.org/10.1021/acs. nanolett.9b00275.
- [20] S. Mishra, G. Catarina, F. Wu, R. Ortiz, D. Jacob, K. Eimre, J. Ma, C. A. Pignedoli, X. Feng, P. Ruffieux, et al., Nature 598, 287 (2021).
- [21] N. Krane, E. Turco, A. Bernhardt, D. Jacob, G. Gandus, D. Passerone, M. Luisier, M. Juríček, R. Fasel, J. Fernández-Rossier, et al., Nano Letters 23, 9353-9359 (2023), ISSN 1530-6992, URL http://dx.doi.org/10.1021/acs.nanolett.3c02633.
- [22] I. Alcón, G. Calogero, N. Papior, A. Antidormi, K. Song, A. W. Cummings, M. Brandbyge, and S. Roche, Journal of the American Chemical Society 144, 8278 (2022), URL https://doi.org/10.1021/jacs.2c02178.
- [23] A. Sil, L. Hamilton, J. M. F. Morris, A. H. S. Daaoub, J. H. H. Burrows, C. M. Robertson, K. Luzyanin, S. J. Higgins, H. Sadeghi, R. J. Nichols, et al., Angewandte Chemie 136 (2024), ISSN 1521-3757, URL http://dx. doi.org/10.1002/ange.202410304.

- [24] B. Lawson, E. Vidal, M. M. Haley, and M. Kamenetska, Extreme anti-ohmic conductance enhancement in neutral diradical acene-like molecular junctions (2024), URL https://arxiv.org/abs/2403.04906.
- [25] C. Herrmann, G. C. Solomon, and M. A. Ratner, Journal of the American Chemical Society 132, 3682 (2010), URL https://doi.org/10.1021/ja910483b.
- [26] R. Frisenda, R. Gaudenzi, C. Franco, M. Mas-Torrent, C. Rovira, J. Veciana, I. Alcon, S. T. Bromley, E. Burzurí, and H. S. J. van der Zant, Nano Letters 15, 3109 (2015), URL https://doi.org/10.1021/acs. nanolett.5b00155.
- [27] Y. Chelli, S. Sandhu, A. H. S. Daaoub, S. Sangtarash, and H. Sadeghi, Nano Letters 23, 3748-3753 (2023), ISSN 1530-6992, URL http://dx.doi.org/10.1021/ acs.nanolett.2c05068.
- [28] Y. Qiu, A. Equbal, C. Lin, Y. Huang, P. J. Brown, R. M. Young, M. D. Krzyaniak, and M. R. Wasielewski, Angewandte Chemie International Edition 62 (2022), ISSN 1521-3773, URL http://dx.doi.org/10.1002/ anie.202214668.
- [29] S. Gorgon, K. Lv, J. Grüne, B. H. Drummond, W. K. Myers, G. Londi, G. Ricci, D. Valverde, C. Tonnelé, P. Murto, et al., Nature 620, 538-544 (2023), ISSN 1476-4687, URL http://dx.doi.org/10.1038/s41586-023-06222-1.
- [30] Y. R. Poh, D. Morozov, N. P. Kazmierczak, R. G. Hadt, G. Groenhof, and J. Yuen-Zhou, Journal of the American Chemical Society 146, 15549-15561 (2024), ISSN 1520-5126, URL http://dx.doi.org/10.1021/ jacs.4c04360.
- [31] S. Sanvito, Chemical Society Reviews 40, 3336 (2011), URL https://doi.org/10.1039/c1cs15047b.
- [32] Y. Ishigaki, T. Harimoto, T. Shimajiri, and T. Suzuki, Chemical Reviews 123, 13952-13965 (2023), ISSN 1520-6890, URL http://dx.doi.org/10.1021/acs. chemrev.3c00376.
- [33] M. Smeu, O. L. A. Monti, and D. McGrath, Physical Chemistry Chemical Physics 23, 24106 (2021), URL https://doi.org/10.1039/d1cp04037e.
- [34] L. Garnier, B. Verlhac, P. Abufager, N. Lorente, M. Ormaza, and L. Limot, Nano Letters 20, 8193-8199 (2020), ISSN 1530-6992, URL http://dx.doi.org/10.1021/acs.nanolett.0c03271.
- [35] F.-K. Yang, J. Cao, T. Zhang, H.-X. Jiang, H.-B. Cui, and K. Wang, ACS Sensors 9, 5445-5453 (2024), ISSN 2379-3694, URL http://dx.doi.org/10.1021/acssensors.4c01665.
- [36] Y. Yonekuta, K. Susuki, K. Oyaizu, K. Honda, and H. Nishide*, Journal of the American Chemical Society 129, 14128–14129 (2007), ISSN 1520-5126, URL http://dx.doi.org/10.1021/ja075553p.
- [37] W. Zeng and J. Wu, Chem 7, 358 (2021), URL https://doi.org/10.1016/j.chempr.2020.10.009.
- [38] L. Yuan, C. Franco, N. Crivillers, M. Mas-Torrent, L. Cao, C. S. S. Sangeeth, C. Rovira, J. Veciana, and C. A. Nijhuis, Nature Communications 7 (2016), URL https://doi.org/10.1038/ncomms12066.
- [39] W. H. Appelt, A. Droghetti, L. Chioncel, M. M. Radonjić, E. Muñoz, S. Kirchner, D. Vollhardt, and I. Rungger, Nanoscale 10, 17738 (2018), URL https://doi.org/10.1039/c8nr03991g.
- [40] H. Zhang and C. Herrmann, The Journal of Physical Chemistry C 127, 19202–19212 (2023), ISSN 1932-7455,

- URL http://dx.doi.org/10.1021/acs.jpcc.3c04401.
- [41] Y. Ji, L. Long, and Y. Zheng, Materials Chemistry Frontiers 4, 3433 (2020), URL https://doi.org/10.1039/ d0qm00122h.
- [42] Y. Jiang, S. Li, Y. Wang, H. Pan, Y. Wang, S. Sanvito, and S. Hou, The Journal of Physical Chemistry C 127, 9268-9277 (2023), ISSN 1932-7455, URL http://dx. doi.org/10.1021/acs.jpcc.3c00224.
- [43] M. Smeu and G. A. DiLabio, The Journal of Physical Chemistry C 114, 17874 (2010), URL https://doi. org/10.1021/jp105589y.
- [44] A. K. Mitchell, K. G. L. Pedersen, P. Hedegård, and J. Paaske, Nature Communications 8 (2017), URL https://doi.org/10.1038/ncomms15210.
- [45] J. P. Bergfield, G. C. Solomon, C. A. Stafford, and M. A. Ratner, Nano Letters 11, 2759 (2011), URL https://doi.org/10.1021/n1201042m.
- [46] D. Hernangómez-Pérez, S. Gunasekaran, L. Venkataraman, and F. Evers, Nano Letters 20, 2615 (2020), URL https://doi.org/10.1021/acs.nanolett.0c00136.
- [47] E. Turco, S. Mishra, J. Melidonie, K. Eimre, S. Obermann, C. A. Pignedoli, R. Fasel, X. Feng, and P. Ruffieux, The journal of physical chemistry letters 12, 8314 (2021).
- [48] D. Jacob and J. Fernández-Rossier, Physical Review B 106 (2022), ISSN 2469-9969, URL http://dx.doi.org/ 10.1103/PhysRevB.106.205405.
- [49] E. Turco, A. Bernhardt, N. Krane, L. Valenta, R. Fasel, M. Juríček, and P. Ruffieux, JACS Au 3, 1358-1364 (2023), ISSN 2691-3704, URL http://dx.doi.org/10. 1021/jacsau.2c00666.
- [50] S. Bhandary, J. M. Tomczak, and A. Valli, Nanoscale Advances 3, 4990 (2021), URL https://doi.org/10. 1039/dlna00407g.
- [51] F. Gao, R. E. Menchón, A. Garcia-Lekue, and M. Brandbyge, Communications Physics 6 (2023), ISSN 2399-3650, URL http://dx.doi.org/10.1038/ s42005-023-01231-y.
- [52] J. P. Perdew, International Journal of Quantum Chemistry 28, 497 (2009), URL https://doi.org/10.1002/qua.560280846.
- [53] M. Sentef, J. Kuneš, P. Werner, and A. P. Kampf, Phys. Rev. B 80, 155116 (2009), URL https://link.aps. org/doi/10.1103/PhysRevB.80.155116.
- [54] F. Hüser, T. Olsen, and K. S. Thygesen, Physical Review B 87 (2013), URL https://doi.org/10.1103/physrevb.87.235132.
- [55] A. Valli, G. Sangiovanni, A. Toschi, and K. Held, Physical Review B 86, 115418 (2012).
- [56] A. Valli, T. Schäfer, P. Thunström, G. Rohringer, S. Andergassen, G. Sangiovanni, K. Held, and A. Toschi, Physical Review B 91 (2015), URL https://doi.org/ 10.1103/physrevb.91.115115.
- [57] A. Valli, A. Amaricci, A. Toschi, T. Saha-Dasgupta, K. Held, and M. Capone, Physical Review B 94 (2016), URL https://doi.org/10.1103/physrevb.94.245146.
- [58] M. Schüler, S. Barthel, T. Wehling, M. Karolak, A. Valli, and G. Sangiovanni, The European Physical Journal Special Topics 226, 2615 (2017), URL https: //doi.org/10.1140/epjst/e2017-70049-3.
- [59] A. Valli, A. Amaricci, V. Brosco, and M. Capone, Nano Letters 18, 2158 (2018), URL https://doi.org/10. 1021/acs.nanolett.8b00453.

- [60] A. Valli, A. Amaricci, V. Brosco, and M. Capone, Physical Review B 100 (2019), URL https://doi.org/10.1103/physrevb.100.075118.
- [61] P. Pudleiner, P. Thunström, A. Valli, A. Kauch, G. Li, and K. Held, Physical Review B 99 (2019), URL https: //doi.org/10.1103/physrevb.99.125111.
- [62] A. Fediai, P. Reiser, J. E. O. Peña, P. Friederich, and W. Wenzel, Scientific Data 10 (2023), ISSN 2052-4463, URL http://dx.doi.org/10.1038/ s41597-023-02486-4.
- [63] H. Park, J. Park, A. K. L. Lim, E. H. Anderson, A. P. Alivisatos, and P. L. McEuen, Nature 407, 57-60 (2000), ISSN 1476-4687, URL http://dx.doi.org/10. 1038/35024031.
- [64] S. Kubatkin, A. Danilov, M. Hjort, J. Cornil, J.-L. Brédas, N. Stuhr-Hansen, P. Hedegård, and T. Bjørnholm, Nature 425, 698-701 (2003), ISSN 1476-4687, URL http://dx.doi.org/10.1038/nature02010.
- [65] M. Poot, E. Osorio, K. O'Neill, J. M. Thijssen, D. Vanmaekelbergh, C. A. van Walree, L. W. Jenneskens, and H. S. J. van der Zant, Nano Letters 6, 1031–1035 (2006), ISSN 1530-6992, URL http://dx.doi.org/10. 1021/nl0604513.
- [66] A. N. Aleshin, H. J. Lee, S. H. Jhang, H. S. Kim, K. Akagi, and Y. W. Park, Physical Review B 72 (2005), ISSN 1550-235X, URL http://dx.doi.org/10.1103/ PhysRevB.72.153202.
- [67] Xu, Xiao, X. Yang, L. Zang, and Tao, Journal of the American Chemical Society 127, 2386-2387 (2005), ISSN 1520-5126, URL http://dx.doi.org/10.1021/ ja042385h.
- [68] H. Song, Y. Kim, Y. H. Jang, H. Jeong, M. A. Reed, and T. Lee, Nature 462, 1039–1043 (2009), ISSN 1476-4687, URL http://dx.doi.org/10.1038/nature08639.
- [69] M. Y. Han, B. Özyilmaz, Y. Zhang, and P. Kim, Physical Review Letters 98 (2007), ISSN 1079-7114, URL http://dx.doi.org/10.1103/PhysRevLett.98. 206805.
- [70] F. Sols, F. Guinea, and A. H. C. Neto, Physical Review Letters 99 (2007), ISSN 1079-7114, URL http://dx. doi.org/10.1103/PhysRevLett.99.166803.
- [71] A. I. Krylov, in Reviews in Computational Chemistry (John Wiley & Sons, Inc., 2017), pp. 151–224, URL https://doi.org/10.1002/9781119356059.ch4.
- [72] D. Jacob, K. Haule, and G. Kotliar, Physical Review B 82 (2010), URL https://doi.org/10.1103/physrevb. 82.195115.
- [73] D. Jacob, Journal of Physics: Condensed Matter 27, 245606 (2015).
- [74] A. Droghetti, M. M. Radonjić, A. Halder, I. Rungger, and L. Chioncel, Physical Review B 105 (2022), URL https://doi.org/10.1103/physrevb.105.115129.
- [75] A. Droghetti, M. M. Radonjić, L. Chioncel, and I. Rungger, Physical Review B 106 (2022), URL https://doi. org/10.1103/physrevb.106.075156.
- [76] C. Lupo, F. Jamet, W. H. T. Tse, I. Rungger, and C. Weber, Nature Computational Science 1, 410–420 (2021), ISSN 2662-8457, URL http://dx.doi.org/10. 1038/s43588-021-00090-3.
- [77] G. D. Scott and D. Natelson, ACS Nano 4, 3560-3579 (2010), ISSN 1936-086X, URL http://dx.doi.org/10. 1021/nn100793s.
- [78] R. Requist, S. Modesti, P. P. Baruselli, A. Smogunov, M. Fabrizio, and E. Tosatti, Proceedings of the National

- Academy of Sciences 111, 69 (2013), URL https://doi.org/10.1073/pnas.1322239111.
- [79] D. Jacob, R. Ortiz, and J. Fernández-Rossier, Physical Review B 104 (2021), ISSN 2469-9969, URL http:// dx.doi.org/10.1103/PhysRevB.104.075404.
- [80] E. Li, B. Danu, Y. Liu, H. Xie, J. W. Y. Lam, B. Z. Tang, S. Wang, F. F. Assaad, and N. Lin, Artificially built kondo chains with organic radicals on metallic surfaces: new model system of heavy fermion quantum criticality (2024), URL https://arxiv.org/abs/2408. 01236
- [81] Q. Du, X. Su, Y. Liu, Y. Jiang, C. Li, K. Yan, R. Ortiz, T. Frederiksen, S. Wang, and P. Yu, Nature Communications 14 (2023), ISSN 2041-1723, URL http://dx.doi.org/10.1038/s41467-023-40542-0.
- [82] L. Zuo, L. Ye, X. Li, R.-X. Xu, Y. Yan, and X. Zheng, The Journal of Physical Chemistry Letters 15, 5761-5769 (2024), ISSN 1948-7185, URL http: //dx.doi.org/10.1021/acs.jpclett.4c01063.
- [83] N. Marzari, A. A. Mostofi, J. R. Yates, I. Souza, and D. Vanderbilt, Reviews of Modern Physics 84, 1419-1475 (2012), ISSN 1539-0756, URL http://dx. doi.org/10.1103/RevModPhys.84.1419.
- [84] V. Vitale, G. Pizzi, A. Marrazzo, J. R. Yates, N. Marzari, and A. A. Mostofi, npj Computational Materials 6 (2020), ISSN 2057-3960, URL http://dx.doi. org/10.1038/s41524-020-0312-y.
- [85] C. Stieger and M. Luisier, Winterface: An interface from wannier90 to quantum transport (2020), URL https://arxiv.org/abs/2007.04268.
- [86] K. S. Thygesen, L. B. Hansen, and K. W. Jacobsen, Physical Review Letters 94 (2005), ISSN 1079-7114, URL http://dx.doi.org/10.1103/PhysRevLett.94. 026405.
- [87] A. Borges and G. C. Solomon, The Journal of Chemical Physics 144 (2016), ISSN 1089-7690, URL http://dx. doi.org/10.1063/1.4950828.
- [88] G. Gandus, A. Valli, D. Passerone, and R. Stadler, The Journal of Chemical Physics 153, 194103 (2020), URL https://doi.org/10.1063/5.0021821.
- [89] A. Borges, J. Xia, S. H. Liu, L. Venkataraman, and G. C. Solomon, Nano Letters 17, 4436-4442 (2017), ISSN 1530-6992, URL http://dx.doi.org/10.1021/ acs.nanolett.7b01592.
- [90] A. Borges, E.-D. Fung, F. Ng, L. Venkataraman, and G. C. Solomon, The Journal of Physical Chemistry Letters 7, 4825–4829 (2016), ISSN 1948-7185, URL http://dx.doi.org/10.1021/acs.jpclett.6b02494.
- [91] P.-O. Löwdin, The Journal of Chemical Physics 18, 365 (1950).
- [92] E. Pavarini, S. Biermann, A. Poteryaev, A. Lichtenstein, A. Georges, and O. Andersen, Physical Review Letters 92, 176403 (2004).
- [93] I. Solovyev, Physical Review B 69, 134403 (2004).
- [94] T. Miyake, F. Aryasetiawan, and M. Imada, Physical Review B 80, 155134 (2009).
- [95] F. Aryasetiawan, K. Karlsson, O. Jepsen, and U. Schönberger, Physical Review B 74, 125106 (2006).
- [96] A. Georges, G. Kotliar, W. Krauth, and M. J. Rozenberg, Reviews of Modern Physics 68, 13 (1996), URL https://doi.org/10.1103/revmodphys.68.13.
- [97] M. Snoek, I. Titvinidze, C. Tőke, K. Byczuk, and W. Hofstetter, New Journal of Physics 10, 093008 (2008), URL https://doi.org/10.1088/1367-2630/

- 10/9/093008.
- [98] A. Valli, G. Sangiovanni, O. Gunnarsson, A. Toschi, and K. Held, Physical Review Letters 104 (2010), URL https://doi.org/10.1103/physrevlett.104.246402.
- [99] A. Valli, H. Das, G. Sangiovanni, T. Saha-Dasgupta, and K. Held, Physical Review B 92 (2015), URL https: //doi.org/10.1103/physrevb.92.115143.
- [100] H. Bruus and K. Flensberg, Many-body quantum theory in condensed matter physics: an introduction (OUP Oxford, 2004).
- [101] E. Gull, A. J. Millis, A. I. Lichtenstein, A. N. Rubtsov, M. Troyer, and P. Werner, Reviews of Modern Physics 83, 349 (2011), URL https://doi.org/10. 1103/revmodphys.83.349.
- [102] M. Jarrell and J. Gubernatis, Physics Reports 269, 133 (1996), URL https://doi.org/10.1016/ 0370-1573(95)00074-7.
- [103] Note1, this approximation neglects non-local interaction terms, which could otherwise be taken into account either at the mean-field level or within alternative implementations, such as extended DMFT [172].
- [104] H. Das, G. Sangiovanni, A. Valli, K. Held, and T. Saha-Dasgupta, 107 (2011), URL https://doi.org/10. 1103/physrevlett.107.197202.
- [105] C. M. Kropf, A. Valli, P. Franceschini, G. L. Celardo, M. Capone, C. Giannetti, and F. Borgonovi, Physical Review B 100 (2019), URL https://doi.org/10. 1103/physrevb.100.035126.
- [106] K. Baumann, A. Valli, A. Amaricci, and M. Capone, Physical Review A 101 (2020), URL https://doi.org/ 10.1103/physreva.101.033611.
- [107] A. Amaricci, A. Valli, G. Sangiovanni, B. Trauzettel, and M. Capone, Physical Review B 98 (2018), URL https://doi.org/10.1103/physrevb.98.045133.
- [108] V. I. Anisimov, J. Zaanen, and O. K. Andersen, Phys. Rev. B 44, 943 (1991), URL https://link.aps.org/doi/10.1103/PhysRevB.44.943.
- [109] M. Czyżyk and G. Sawatzky, Physical Review B 49, 14211 (1994).
- [110] M. Karolak, G. Ulm, T. Wehling, V. Mazurenko, A. Poteryaev, and A. Lichtenstein, Journal of Electron Spectroscopy and Related Phenomena 181, 11 (2010), URL https://doi.org/10.1016/j.elspec. 2010.05.021.
- [111] V. I. Anisimov, F. Aryasetiawan, and A. Lichtenstein, Journal of Physics: Condensed Matter 9, 767 (1997).
- [112] A. Petukhov, I. Mazin, L. Chioncel, and A. Lichtenstein, Physical Review B 67, 153106 (2003).
- [113] G. Kotliar, S. Y. Savrasov, K. Haule, V. S. Oudovenko, O. Parcollet, and C. A. Marianetti, Rev. Mod. Phys. 78, 865 (2006), URL https://link.aps.org/doi/10. 1103/RevModPhys.78.865.
- [114] K. Held, Advances in Physics 56, 829 (2007), URL https://doi.org/10.1080/00018730701619647.
- [115] A. Liechtenstein, V. I. Anisimov, and J. Zaanen, Physical Review B 52, R5467 (1995).
- [116] V. I. Anisimov, I. Solovyev, M. Korotin, M. Czyżyk, and G. Sawatzky, Physical Review B 48, 16929 (1993).
- [117] I. Solovyev, P. Dederichs, and V. Anisimov, Physical Review B 50, 16861 (1994).
- [118] M. Karolak, G. Ulm, T. Wehling, V. Mazurenko, A. Poteryaev, and A. Lichtenstein, Journal of Electron Spectroscopy and Related Phenomena 181, 11–15 (2010), ISSN 0368-2048, URL http://dx.doi.org/10.

- 1016/j.elspec.2010.05.021.
- [119] S. Datta, Quantum transport: atom to transistor (Cambridge university press, 2005).
- [120] D. A. Ryndyk et al., Springer Series in Solid-State Sciences 184 (2016).
- [121] G. Gandus, Y. Lee, L. Deuschle, D. Passerone, and M. Luisier, Solid-State Electronics 199, 108499 (2023), ISSN 0038-1101, URL http://dx.doi.org/10.1016/j. sse.2022.108499.
- [122] Y. Meir and N. S. Wingreen, Physical Review Letters 68, 2512 (1992).
- [123] A. Ferretti, A. Calzolari, R. Di Felice, and F. Manghi, Physical Review B 72, 125114 (2005).
- [124] T.-K. Ng, Physical Review Letters 76, 487 (1996).
- [125] N. Sergueev, Q.-f. Sun, H. Guo, B. Wang, and J. Wang, Physical Review B 65, 165303 (2002).
- [126] H. Ness, L. K. Dash, and R. W. Godby, Physical Review B 82 (2010), ISSN 1550-235X, URL http://dx.doi. org/10.1103/physrevb.82.085426.
- [127] A. Oguri, Journal of the Physical Society of Japan 70, 2666-2681 (2001), ISSN 1347-4073, URL http://dx. doi.org/10.1143/jpsj.70.2666.
- [128] W. F. dos Santos, F. Amorim, and A. Reily Rocha, Nanotechnology 36, 025201 (2024), ISSN 1361-6528, URL http://dx.doi.org/10.1088/1361-6528/ad83da.
- [129] A. H. Larsen, J. J. Mortensen, J. Blomqvist, I. E. Castelli, R. Christensen, M. Dułak, J. Friis, M. N. Groves, B. Hammer, C. Hargus, et al., Journal of Physics: Condensed Matter 29, 273002 (2017), URL http://stacks.iop.org/0953-8984/29/i=27/a=273002.
- [130] J. J. Mortensen, L. B. Hansen, and K. W. Jacobsen, Phys. Rev. B 71, 035109 (2005), URL https://link. aps.org/doi/10.1103/PhysRevB.71.035109.
- [131] A. H. Larsen, M. Vanin, J. J. Mortensen, K. S. Thygesen, and K. W. Jacobsen, Phys. Rev. B 80, 195112 (2009), URL https://link.aps.org/doi/10. 1103/PhysRevB.80.195112.
- [132] J. Enkovaara, C. Rostgaard, J. J. Mortensen, J. Chen, M. Dułak, L. Ferrighi, J. Gavnholt, C. Glinsvad, V. Haikola, H. A. Hansen, et al., Journal of Physics: Condensed Matter 22, 253202 (2010).
- [133] J. P. Perdew, K. Burke, and M. Ernzerhof, Phys. Rev. Lett. 77, 3865 (1996), URL https://link.aps.org/doi/10.1103/PhysRevLett.77.3865.
- [134] A. Amaricci, L. Crippa, A. Scazzola, F. Petocchi, G. Mazza, L. de Medici, and M. Capone, Computer Physics Communications 273, 108261 (2022), ISSN 0010-4655, URL http://dx.doi.org/10.1016/j.cpc. 2021.108261.
- [135] L. Crippa, I. Krivenko, S. Giuli, G. Bellomia, A. Kowalski, F. Petocchi, A. Scazzola, M. Wallerberger, G. Mazza, L. de' Medici, et al., SciPost Physics Codebases (2025), ISSN 2949-804X, URL http://dx.doi.org/10.21468/SciPostPhysCodeb.58.
- [136] G. Gandus, edpty, https://github.com/gandusgui/edpyt.git (2022).
- [137] G. Guido, qtpyt, https://github.com/gandusgui/ qtpyt.git (2022).
- [138] K. B. Clark, P. N. Culshaw, D. Griller, F. P. Lossing, J. A. M. Simoes, and J. C. Walton, The Journal of Organic Chemistry 56, 5535 (1991), URL https://doi.org/10.1021/jo00019a012.

- [139] N. Chalyavi, G. B. Bacskay, A. S. Menon, T. P. Troy, N. J. L. K. Davis, L. Radom, S. A. Reid, and T. W. Schmidt, The Journal of Chemical Physics 135, 124306 (2011), URL https://doi.org/10.1063/1.3640475.
- [140] C. Herrmann, G. C. Solomon, and M. A. Ratner, The Journal of Chemical Physics 134, 224306 (2011), URL https://doi.org/10.1063/1.3598519.
- [141] L. Hedin, Physical Review 139, A796 (1965), URL https://doi.org/10.1103/physrev.139.a796.
- [142] F. Aryasetiawan and O. Gunnarsson, Reports on Progress in Physics 61, 237 (1998), URL https://doi. org/10.1088/0034-4885/61/3/002.
- [143] A. Stan, N. E. Dahlen, and R. van Leeuwen, Europhysics Letters (EPL) 76, 298 (2006), URL https: //doi.org/10.1209/epl/i2006-10266-6.
- [144] J. B. Neaton, M. S. Hybertsen, and S. G. Louie, Physical Review Letters 97 (2006), URL https://doi.org/10. 1103/physrevlett.97.216405.
- [145] K. S. Thygesen and A. Rubio, The Journal of Chemical Physics 126, 091101 (2007), URL https://doi.org/ 10.1063/1.2565690.
- [146] K. S. Thygesen and A. Rubio, Physical Review B 77 (2008), URL https://doi.org/10.1103/physrevb.77. 115333.
- [147] C. Rostgaard, K. W. Jacobsen, and K. S. Thygesen, Physical Review B 81 (2010), URL https://doi.org/ 10.1103/physrevb.81.085103.
- [148] M. Strange, C. Rostgaard, H. Häkkinen, and K. S. Thygesen, Physical Review B 83 (2011), URL https: //doi.org/10.1103/physrevb.83.115108.
- [149] M. Mansouri, D. Casanova, P. Koval, and D. Sánchez-Portal, New Journal of Physics 23, 093027 (2021), URL https://doi.org/10.1088/1367-2630/ac1bf3.
- [150] K. Held, C. Taranto, G. Rohringer, and A. Toschi, Forschungszentrum Juelich GmbH pp. 1–22 (2011).
- [151] C. R. Arroyo, S. Tarkuc, R. Frisenda, J. S. Seldenthuis, C. H. M. Woerde, R. Eelkema, F. C. Grozema, and H. S. J. van der Zant, Angewandte Chemie 125, 3234 (2013), URL https://doi.org/10.1002/ange.201207667.
- [152] G. Yang, H. Wu, J. Wei, J. Zheng, Z. Chen, J. Liu, J. Shi, Y. Yang, and W. Hong, Chinese Chemical Letters 29, 147 (2018), URL https://doi.org/10.1016/ j.cclet.2017.06.015.
- [153] Y. Li, M. Buerkle, G. Li, A. Rostamian, H. Wang, Z. Wang, D. R. Bowler, T. Miyazaki, L. Xiang, Y. Asai, et al., Nature Materials 18, 357 (2019), URL https: //doi.org/10.1038/s41563-018-0280-5.
- [154] P. Sautet and C. Joachim, Chemical Physics Letters 153, 511 (1988), URL https://doi.org/10.1016/0009-2614(88)85252-7.
- [155] G. C. Solomon, D. Q. Andrews, T. Hansen, R. H. Goldsmith, M. R. Wasielewski, R. P. V. Duyne, and M. A. Ratner, The Journal of Chemical Physics 129, 054701 (2008), URL https://doi.org/10.1063/1.2958275.
- [156] P. Sam-ang and M. G. Reuter, New Journal of Physics 19, 053002 (2017), URL https://doi.org/10.1088/

- 1367-2630/aa6c23.
- [157] D. Nozaki and C. Toher, The Journal of Physical Chemistry C 121, 11739 (2017), URL https://doi.org/10.1021/acs.jpcc.6b11951.
- [158] S. Gunasekaran, J. E. Greenwald, and L. Venkataraman, Nano Letters 20, 2843 (2020), URL https://doi. org/10.1021/acs.nanolett.0c00605.
- [159] Y.-F. Zhou, W.-Y. Chang, J.-Z. Chen, J.-R. Huang, J.-Y. Fu, J.-N. Zhang, L.-Q. Pei, Y.-H. Wang, S. Jin, and X.-S. Zhou, Nanotechnology 33, 095201 (2021), URL https://doi.org/10.1088/1361-6528/ac3b84.
- [160] J. Prasongkit and A. R. Rocha, RSC Advances 6, 59299 (2016).
- [161] O. Sengul, J. Völkle, A. Valli, and R. Stadler, Phys. Rev. B 105, 165428 (2022), URL https://link.aps. org/doi/10.1103/PhysRevB.105.165428.
- [162] U. Fano, Physical Review 124, 1866 (1961), URL https://doi.org/10.1103/physrev.124.1866.
- [163] A. E. Miroshnichenko, S. Flach, and Y. S. Kivshar, Reviews of Modern Physics 82, 2257 (2010), URL https://doi.org/10.1103/revmodphys.82.2257.
- [164] Y. Zheng, P. Duan, Y. Zhou, C. Li, D. Zhou, Y. Wang, L.-C. Chen, Z. Zhu, X. Li, J. Bai, et al., Angewandte Chemie International Edition 61 (2022), URL https: //doi.org/10.1002/anie.202210097.
- [165] T. T. Phùng, R. Peters, A. Honecker, G. T. de Laissardière, and J. Vahedi, Physical Review B 102 (2020), URL https://doi.org/10.1103/physrevb. 102.035160.
- [166] O. Sengul, A. Valli, and R. Stadler, Nanoscale 13, 17011-17021 (2021), ISSN 2040-3372, URL http://dx. doi.org/10.1039/D1NR01230D.
- [167] S. Mishra, D. Beyer, K. Eimre, S. Kezilebieke, R. Berger, O. Gröning, C. A. Pignedoli, K. Müllen, P. Liljeroth, P. Ruffieux, et al., Nature nanotechnology 15, 22 (2020).
- [168] A. Valli and J. M. Tomczak, Journal of Computational Electronics 22, 1363-1376 (2023), ISSN 1572-8137, URL http://dx.doi.org/10.1007/s10825-023-02043-7.
- [169] A. Valli, T. Fabian, F. Libisch, and R. Stadler, Carbon 214, 118358 (2023), ISSN 0008-6223, URL http://dx. doi.org/10.1016/j.carbon.2023.118358.
- [170] C. M. Guédon, H. Valkenier, T. Markussen, K. S. Thygesen, J. C. Hummelen, and S. J. van der Molen, Nature Nanotechnology 7, 305-309 (2012), ISSN 1748-3395, URL http://dx.doi.org/10.1038/nnano.2012. 37
- [171] J. E. Greenwald, J. Cameron, N. J. Findlay, T. Fu, S. Gunasekaran, P. J. Skabara, and L. Venkataraman, Nature Nanotechnology 16, 313-317 (2020), ISSN 1748-3395, URL http://dx.doi.org/10.1038/ s41565-020-00807-x.
- [172] P. Sun and G. Kotliar, Physical Review B 66 (2002), ISSN 1095-3795, URL http://dx.doi.org/10.1103/ PhysRevB.66.085120.